containing DPPA4 was resistant to MNase digestion when compared to that without DPPA4. These findings imply that DPPA4 modulates the chromatin structure in ES cells and raises the possibility that DPPA4 is involved in the maintenance of unique chromatin states of ES cell. Thus, elucidating the function of DPPA4 potentially facilitates revealing novel properties of unique chromatin states of ES cells.

Experimental procedures

ES cell culture

The mouse ES cell line, MGZRTcH2 (Masui *et al.* 2005), was maintained in ES medium consisting of Knockout DMEM (Gibco Life Technologies, Carlsbad, CA, USA) containing 1% embryonic stem cell screened fetal bovine serum (FBS; Hyclone Thermo Fisher Scientific, Waltham, MA, USA), 10% Knockout Serum Replacement (KSR), 2 mM L-glutamine, 100 U/mL penicillin, 100 μg/mL streptomycin, 100 μM MEM non-essential amino acids solution (Gibco Life Technologies), 0.3 mM monothioglycerol (Sigma-Aldrich, St. Louis, MO, USA), and 1000 U/mL LIF (Millipore, Billerica, MA, USA) on gelatin-coated dishes.

Immunocytochemistry and Western blotting

Immunocytochemistry and Western blotting were performed as described (Masaki *et al.* 2007). The following primary antibodies were used: DPPA4 (Masaki *et al.* 2007); GFP (GF090R; Nacalai Tesque, Kyoto, Japan); histone H1 (AE-4; Santa Cruz Biotechnology, Santa Cruz, CA, USA); histone H2A (Active Motif, Carlsbad, CA, USA); histone H2B (Active Motif); histone H3 (ab1791, Abcam, Cambridge, UK); histone H4 (Active Motif); β-actin (AC-74, Sigma); and 6xHis (A190-114A, BETHYL Laboratories, Montgomery, USA).

FRAP analysis

The mouse DPPA4, DPPA4ΔC (1-348), DPPA4ΔN (349-888), histone $H1^0$, and histone H3 cDNAs were subcloned into pBlueScript II SK+ (pBS) vector (Stratagene Agilent Technologies, Santa Clara, CA, USA). Each cDNA in the plasmid was excised and ligated into EGFP fusion protein expression vector, pEGFP-N1 (Clontech Takara Bio, Shiga, Japan). These vectors were transfected into ES cells with lipofectamine2000 (Invitrogen Life Technologies, Carlsbad, CA, USA), and transfected ES cells were plated on gelatin-coated glass bottom dishes (Matsunami, Osaka, Japan) 24 h after transfection. The next day, the culture medium was changed to ES cell medium containing Leibovitz L-15 medium (Gibco Life Technologies) instead of Knockout DMEM. FRAP experiments were performed with a LSM 510 META confocal microscope (Carl Zeiss, Oberkochen, Germany). The pre-bleach image was collected, followed by a 500-ms bleach pulse with a spot 4 μm in diameter. Bleaching was performed with the 488-nm line of a 25 mW argon laser set to 100%. Single images were collected with the 488-nm line of the argon laser (set to 5%) every 1 s for 120 s. FRAP recovery curves were created from images with the background subtracted. Total fluorescence was determined for each image and compared to the total pre-bleach fluorescence to determine the amount of fluorescence lost during the imaging. The fluorescence intensity in the bleached area was normalized to the initial fluorescence in the bleached area.

Preparation and purification of proteins

Subcloned cDNAs of mouse DPPA4, DPPA4ΔC, DPPA4ΔN, and histone $H1^0$ were inserted into pET21a+ (Novagen Merck, Darmstadt, Germany). *E. coli* BL21(DE3) cells were transformed with each vector, and protein expression was induced by 100 μM isopropyl beta-D-1-thiogalactopyranoside at 30 °C for 2 h. The cells were treated with lysis buffer [20 mM Tris-HCl, 500 mM NaCl, 1% NP-40, 1 mg/mL lysozyme, 5% glycerol, and protease inhibitor cocktail (PIC; Roche Diagnostic, Basel, Switzerland)] and sonicated. The whole extract was centrifuged at 15 000 g for 30 min. Using supernatant, recombinant proteins were purified by TALON metal affinity resin (Clontech Takara Bio) according to the manufacturer's instructions. Core histone proteins were purified from mouse ES cells by histone purification kit (Active Motif) according to the manufacturer's instructions. The purity of these proteins was confirmed by SDS-PAGE and coomassie brilliant blue staining.

Gel shift assay

pBS plasmid DNA (100 ng) was incubated with 100, 200, 400, or 800 ng purified DPPA4-His_6, DPPA4ΔC-His_6, or DPPA4ΔN-His_6 proteins on ice for 30 min in 60 mM NaCl, 50 mM $NaHPO_4$, 2 mM EDTA, 10% glycerol, and 2 mg/mL BSA. The samples were electrophoresed on a 1% agarose gel, and the DNA visualized by ethidium bromide staining. To obtain methylated pBS plasmid DNA, CpG methylase (*Sss* I Methylase; New England Biolabs, Ipswich, MA, USA) was used.

Far-Western blot analysis

Far-Western blotting was carried out as described by Wu *et al.* 2007. Briefly, 250 ng of each purified core histone was separated by SDS-PAGE and transferred to a nitrocellulose membrane. Proteins on the membrane were denatured and renatured by gradually reducing the guanidine-HCl concentration. After blocking with 5% non-fat dry milk, the membrane was incubated with purified DPPA4-His_6 (500 ng/mL) in blocking reagent followed by detection with anti-DPPA4 antibodies.

Co-immunoprecipitation

ES cells were washed with PBS, resuspended in buffer C (20 mM Tris-HCl, 150 mM NaCl, 2 mM EDTA, 0.1% Tween20, and PIC), and incubated on ice for 20 min. The lysate was robustly sonicated and centrifuged for 30 min at 16 000 g. The supernatant was incubated overnight with anti-DPPA4 antibodies or control IgG (10 μg), and then incubated with protein G Sepharose (GE Healthcare, Waukesha, WI, USA) for 1 h at 4 °C. The beads were washed three times with buffer B (20 mM Tris-HCl, 150 mM NaCl, 0.1% Tween20, 0.5 mM EDTA, 10% glycerol, and PIC) followed by boiling with SDS sample buffer (50 mM Tris-HCl, pH 6.8, 2% SDS, 10% glycerol, 2% 2-mercaptoethanol, and 0.2% bromphenolblue). For *in vitro* co-immunoprecipitation, purified histone H2A + H2B (5 μg), histone H3 + H4 (5 μg) or total core histones (10 μg) and recombinant DPPA4-His_6 (1.5 μg), DPPA4ΔC-His_6 or DPPA4ΔN-His_6 (equimolar amount to DPPA4-His_6) proteins were incubated in buffer B for 1 h at 4 °C. Anti-DPPA4 antibodies or control IgG (10 μg) were added to each mixture followed by overnight incubation. The mixtures were then incubated with protein G Sepharose beads blocked with 5% non-fat dry milk for 1 h at 4 °C. The beads were washed three times with buffer B and boiled in SDS sample buffer. These samples were subjected to SDS-PAGE and Western blot analysis using rabbit TrueBlot (eBioscience, San Diego, CA, USA) as secondary antibodies.

Chromatin reconstitution

In vitro reconstituted chromatin was prepared by using mouse ES cell core histones, pBS plasmid DNA, and chromatin assembly kit (Active Motif) according to the manufacturer's instructions. Subsequent to chromatin assembly, either DPPA4-His_6, DPPA4ΔC-His_6, DPPA4ΔN-His_6, $H1^0$-His_6 or BSA was added to the reconstituted chromatin at a ratio of one molecule per nucleosome, and the chromatin mixtures were incubated for 1 h at 27 °C. The chromatin mixtures were digested with several concentrations of enzymatic shearing cocktail containing MNase (chromatin assembly kit) for 5 min, subsequently EDTA and proteinase K (Sigma-Aldrich) were added to the mixtures to stop digestion, and incubated overnight. The mixtures were electrophoresed on a 1.5% agarose gel, and the DNA was visualized by ethidium bromide.

Acknowledgement

This work was supported in part by Grants-in-Aid from Japan Society for the Promotion of Science for JSPS Fellows and for Exploratory Research (20659047).

References

Aravind, L. & Koonin, E.V. (2000) SAP - a putative DNA-binding motif involved in chromosomal organization. *Trends Biochem. Sci.* **25**, 112–114.

Azuara, V., Perry, P., Sauer, S., Spivakov, M., Jørgensen, H.F., John, R.M., Gouti, M., Casanova, M., Warnes, G., Merkenschlager, M. & Fisher, A.G. (2006) Chromatin signatures of pluripotent cell lines. *Nat. Cell Biol.* **8**, 532–538.

Bernstein, B.E., Mikkelsen, T.S., Xie, X., Kamal, M., Huebert, D.J., Cuff, J., Fry, B., Meissner, A., Wernig, M., Plath, K., Jaenisch, R., Wagschal, A., Feil, R., Schreiber, S.L. & Lander, E.S. (2006) A bivalent chromatin structure marks key developmental genes in embryonic stem cells. *Cell* **125**, 315–326.

Boiani, M. & Schöler, H.R. (2005) Regulatory networks in embryo-derived pluripotent stem cells. *Nat. Rev. Mol. Cell Biol.* **6**, 872–884.

van den Boom, V., Kooistra, S.M., Boesjes, M., Geverts, B., Houtsmuller, A.B., Monzen, K., Komuro, I., Essers, J., Drenth-Diephuis, L.J. & Eggen, B.J. (2007) UTF1 is a chromatin-associated protein involved in ES cell differentiation. *J. Cell Biol.* **178**, 913–924.

Bortvin, A., Eggan, K., Skaletsky, H., Akutsu, H., Berry, D.L., Yanagimachi, R., Page, D.C. & Jaenisch, R. (2003) Incomplete reactivation of Oct4-related genes in mouse embryos cloned from somatic nuclei. *Development* **130**, 1673–1680.

Boyer, L.A., Lee, T.I., Cole, M.F., Johnstone, S.E., Levine, S.S., Zucker, J.P., Guenther, M.G., Kumar, R.M., Murray, H.L., Jenner, R.G., Gifford, D.K., Melton, D.A., Jaenisch, R. & Young, R.A. (2005) Core transcriptional regulatory circuitry in human embryonic stem cells. *Cell* **122**, 947–956.

Boyer, L.A., Plath, K., Zeitlinger, J., *et al.* (2006) Polycomb complexes repress developmental regulators in murine embryonic stem cells. *Nature* **441**, 349–353.

Burdon, T., Smith, A. & Savatier, P. (2002) Signaling, cell cycle and pluripotency in embryonic stem cells. *Trends Cell Biol.* **12**, 432–438.

Chakravarthy, H., Boer, B., Desler, M., Mallanna, S.K., McKeithan, T.W. & Rizzino, A. (2008) Identification of DPPA4 and other genes as putative Sox2:Oct-3/4 target genes using a combination of in silico analysis and transcription-based assays. *J. Cell. Physiol.* **216**, 651–662.

Chambers, I., Colby, D., Robertson, M., Nichols, J., Lee, S., Tweedie, S. & Smith, A. (2003) Functional expression cloning of Nanog, a pluripotency sustaining factor in embryonic stem cells. *Cell* **113**, 643–655.

Fan, Y., Nikitina, T., Zhao, J., Fleury, T.J., Bhattacharyya, R., Bouhassira, E.E., Stein, A., Woodcock, C.L. & Skoultchi, A.I. (2005) Histone H1 depletion in mammals alters global chromatin structure but causes specific changes in gene regulation. *Cell* **123**, 1199–1212.

Gaspar-Maia, A., Alajem, A., Polesso, F., Sridharan, R., Mason, M.J., Heidersbach, A., Ramalho-Santos, J., McManus, M.T., Plath, K., Meshorer, E. & Ramalho-Santos, M. (2009) Chd1 regulates open chromatin and pluripotency of embryonic stem cells. *Nature* **460**, 863–868.

Hamatani, T., Carter, M.G., Sharov, A.A. & Ko, M.S. (2004) Dynamics of global gene expression changes during mouse preimplantation development. *Dev. Cell* **6**, 117–131.

Ho, L., Ronan, J.L., Wu, J., Staahl, B.T., Chen, L., Kuo, A., Lessard, J., Nesvizhskii, A.I., Ranish, J. & Crabtree, G.R. (2009) An embryonic stem cell chromatin remodeling complex, esBAF, is essential for embryonic stem cell self-renewal and pluripotency. *Proc. Natl Acad. Sci. USA* **106**, 5181–5186.

Ivanova, N., Dobrin, R., Lu, R., Kotenko, I., Levorse, J., DeCoste, C., Schafer, X., Lun, Y. & Lemischka, I.R. (2006) Dissecting self-renewal in stem cells with RNA interference. *Nature* **442**, 533–538.

Jiang, J., Chan, Y.S., Loh, Y.H., Cai, J., Tong, G.Q., Lim, C.A., Robson, P., Zhong, S. & Ng, H.H. (2008) A core Klf circuitry regulates self-renewal of embryonic stem cells. *Nat. Cell Biol.* **10**, 353–360.

Keller, G. (2005) Embryonic stem cell differentiation: emergence of a new era in biology and medicine. *Genes Dev.* **19**, 1129–1155.

Kim, M.Y., Mauro, S., Gévry, N., Lis, J.T. & Kraus, W.L. (2004) NAD^+-dependent modulation of chromatin structure and transcription by nucleosome binding properties of PARP-1. *Cell* **119**, 803–814.

Lee, T.I., Jenner, R.G., Boyer, L.A., *et al.* (2006) Control of developmental regulators by Polycomb in human embryonic stem cells. *Cell* **125**, 301–313.

Madan, B., Madan, V., Weber, O., Tropel, P., Blum, C., Kieffer, E., Viville, S. & Fehling, H.J. (2009) The pluripotency-associated gene Dppa4 is dispensable for embryonic stem cell identity and germ cell development but essential for embryogenesis. *Mol. Cell. Biol.* **29**, 3186–3203.

Maldonado-Saldivia, J., van den Bergen, J., Krouskos, M., Gilchrist, M., Lee, C., Li, R., Sinclair, A.H., Surani, M.A. & Western, P.S. (2007) Dppa2 and Dppa4 are closely linked SAP motif genes restricted to pluripotent cells and the germ line. *Stem Cells* **25**, 19–28.

Masaki, H., Nishida, T., Kitajima, S., Asahina, K. & Teraoka, H. (2007) Developmental pluripotency-associated 4 (DPPA4) localized in active chromatin inhibits mouse embryonic stem cell differentiation into a primitive ectoderm lineage. *J. Biol. Chem.* **282**, 33034–33042.

Masui, S., Nakatake, Y., Toyooka, Y., Shimosato, D., Yagi, R., Takahashi, K., Okochi, H., Okuda, A., Matoba, R., Sharov, A.A., Ko, M.S. & Niwa, H. (2007) Pluripotency governed by Sox2 via regulation of Oct3/4 expression in mouse embryonic stem cells. *Nat. Cell Biol.* **9**, 625–635.

Masui, S., Shimosato, D., Toyooka, Y., Yagi, R., Takahashi, K. & Niwa, H. (2005) An efficient system to establish multiple embryonic stem cell lines carrying an inducible expression unit. *Nucleic Acids Res.* **33**, e43.

Meshorer, E., Yellajoshula, D., George, E., Scambler, P.J., Brown, D.T. & Misteli, T. (2006) Hyperdynamic plasticity of chromatin proteins in pluripotent embryonic stem cells. *Dev. Cell* **10**, 105–116.

Mitsui, K., Tokuzawa, Y., Itoh, H., Segawa, K., Murakami, M., Takahashi, K., Maruyama, M., Maeda, M. & Yamanaka, S. (2003) The homeoprotein Nanog is required for maintenance of pluripotency in mouse epiblast and ES cells. *Cell* **113**, 631–642.

Nakamura, T., Arai, Y., Umehara, H., Masuhara, M., Kimura, T., Taniguchi, H., Sekimoto, T., Ikawa, M., Yoneda, Y., Okabe, M., Tanaka, S., Shiota, K. & Nakano, T. (2007) PGC7/Stella protects against DNA demethylation in early embryogenesis. *Nat. Cell Biol.* **9**, 64–71.

Niwa, H., Ogawa, K., Shimosato, D. & Adachi, K. (2009) A parallel circuit of LIF signalling pathways maintains pluripotency of mouse ES cells. *Nature* **460**, 118–122.

Niwa, H., Toyooka, Y., Shimosato, D., Strumpf, D., Takahashi, K., Yagi, R. & Rossant, J. (2005) Interaction between Oct3/4 and Cdx2 determines trophectoderm differentiation. *Cell* **123**, 917–929.

Phair, R.D., Scaffidi, P., Elbi, C., Vecerová, J., Dey, A., Ozato, K., Brown, D.T., Hager, G., Bustin, M. & Misteli, T. (2004) Global nature of dynamic protein-chromatin interactions in vivo: three-dimensional genome scanning and dynamic interaction networks of chromatin proteins. *Mol. Cell. Biol.* **24**, 6393–6402.

Siegel, D., Schuff, M., Oswald, F., Cao, Y. & Knöchel, W. (2009) Functional dissection of XDppa2/4 structural domains in Xenopus development. *Mech. Dev.* **126**, 974–989.

Spivakov, M. & Fisher, A.G. (2007) Epigenetic signature of stem-cell identity. *Nat. Rev. Genet.* **8**, 263–271.

Szutorisz, H., Georgiou, A., Tora, L. & Dillon, N. (2006) The Proteasome restricts permissive transcription at tissue-specific gene loci in embryonic stem cells. *Cell* **127**, 1375–1388.

Takahashi, K., Tanabe, K., Ohnuki, M., Narita, M., Ichisaka, T., Tomoda, K. & Yamanaka, S. (2007) Induction of pluripotent stem cells from adult human fibroblasts by defined factors. *Cell* **131**, 861–872.

Thomson, J.A., Itskovitz-Eldor, J., Shapiro, S.S., Waknitz, M.A., Swiergiel, J.J., Marshall, V.S. & Jones, J.M. (1998) Embryonic stem cell lines derived from human blastocysts. *Science* **282**, 1145–1147.

Wu, Y., Li, Q. & Chen, X.Z. (2007) Detecting protein-protein interactions by far western blotting. *Nat. Protoc.* **2**, 3278–3284.

Yu, J., Vodyanik, M.A., Smuga-Otto, K., Antosiewicz-Bourget, J., Frane, J.L., Tian, S., Nie, J., Jonsdottir, G.A., Ruotti, V., Stewart, R., Slukvin, I.I. & Thomson, J.A. (2007) Induced pluripotent stem cell lines derived from human somatic cells. *Science* **318**, 1917–1920.

Zhang, J., Tam, W.L., Tong, G.Q., Wu, Q., Chan, H.Y., Soh, B.S., Lou, Y., Yang, J., Ma, Y., Chai, L., Ng, H.H., Lufkin, T., Robson, P. & Lim, B. (2006) Sall4 modulates embryonic stem cell pluripotency and early embryonic development by the transcriptional regulation of Pou5f1. *Nat. Cell Biol.* **8**, 1114–1123.

Received: 6 October 2009
Accepted: 23 December 2009

THE JOURNAL OF BIOLOGICAL CHEMISTRY VOL. 285, NO. 20, pp. 15201–15208, May 14, 2010

Transcription-dependent Activation of Ataxia Telangiectasia Mutated Prevents DNA-dependent Protein Kinase-mediated Cell Death in Response to Topoisomerase I Poison*[S]

Received for publication, January 6, 2010, and in revised form, March 18, 2010. Published, JBC Papers in Press, March 19, 2010, DOI 10.1074/jbc.M110.101808

Ryo Sakasai[‡1], **Hirobumi Teraoka**[‡], **Masatoshi Takagi**[§], **and Randal S. Tibbetts**[¶]

From the [‡]*Department of Pathological Biochemistry, Medical Research Institute, Tokyo Medical and Dental University, Tokyo 101-0062, Japan, the* [§]*Department of Pediatrics and Developmental Biology, Tokyo Medical and Dental University, Tokyo 113-8519, Japan, and the* [¶]*Department of Pharmacology, University of Wisconsin School of Medicine and Public Health, Madison, Wisconsin 53706*

Camptothecin (CPT) is a topoisomerase I inhibitor, derivatives of which are being used for cancer chemotherapy. CPT-induced DNA double-strand breaks (DSBs) are considered a major cause of its tumoricidal activity, and it has been shown that CPT induces DNA damage signaling through the phosphatidylinositol 3-kinase-related kinases, including ATM (ataxia telangiectasia mutated), ATR (ATM and Rad3-related), and DNA-PK (DNA-dependent protein kinase). In addition, CPT causes DNA strand breaks mediated by transcription, although the downstream signaling events are less well characterized. In this study, we show that CPT-induced activation of ATM requires transcription. Mechanistically, transcription inhibition suppressed CPT-dependent activation of ATM and blocked recruitment of the DNA damage mediator p53-binding protein 1 (53BP1) to DNA damage sites, whereas ATM inhibition abrogated CPT-induced G_1/S and S phase checkpoints. Functional inactivation of ATM resulted in DNA replication-dependent hyperactivation of DNA-PK in CPT-treated cells and dramatic CPT hypersensitivity. On the other hand, simultaneous inhibition of ATM and DNA-PK partially restored CPT resistance, suggesting that activation of DNA-PK is proapoptotic in the absence of ATM. Correspondingly, comet assay and cell cycle synchronization experiments suggested that transcription collapse occurring as the result of CPT treatment are converted to frank double-strand breaks when ATM-deficient cells bypass the G_1/S checkpoint. Thus, ATM suppresses DNA-PK-dependent cell death in response to topoisomerase poisons, a finding with potential clinical implications.

The topoisomerase I (TopI)[2] poison camptothecin (CPT) and its clinically relevant derivatives, topotecan and irinotecan, have been intensively studies for their tumoricidal properties. The molecular target of CPT is TopI, an enzyme that mediates the relaxation of supercoiled DNA (1). This is achieved through the transient introduction of a DNA single-strand break that permits the rotational relaxation of double-stranded DNA. The TopI reaction cycle involves the formation of a transient phosphotyrosyl bond between Tyr^{723} of the enzyme active site and a 3′ DNA end. CPT stabilizes covalent TopI-DNA cleavage complexes (TopI-cc), which are converted into DNA double-strand breaks (DSBs) upon encountering active DNA replication forks (1).

The signaling and repair of CPT-mediated damage have been the focus of intensive research. CPT-induced DSBs possess a single DNA double-strand end (DSE) that is generally not an efficient substrate for nonhomologous end joining DSB repair, which is mediated by DNA-dependent protein kinase (DNA-PK) composed of DNA-PKcs and Ku protein. Instead, CPT-induced DSEs are repaired by homologous recombination (HR) repair, which utilizes a sister chromatid and primes restart of the obstructed DNA replication fork (2, 3). CPT-induced DSEs strongly activate cell cycle checkpoint pathways downstream of the ATM (ataxia telangiectasia mutated) and ATR (ATM and Rad3-related) protein kinases. CPT-induced damage in S phase activates the ATR-Chk1 pathway that mediates S phase arrest (4). Consistent with these important S phase functions, ATR- or Chk1-deficient cells are exquisitely sensitive to TopI poisons (4, 5).

In addition to replication-mediated DNA damage, TopI-cc pose a block to processive RNA polymerase complexes, and the collision of RNA polymerase with TopI-cc results in transcription-mediated DNA damage (6). Although the mechanisms of transcription-coupled damage and signaling are not well understood, recent studies suggest a new role for the ATM protein kinase. CPT-induced activation of ATM is suppressed by inhibitors of transcription, and it has been proposed that ATM responds to RNA-DNA hybrid R-loops that form at stalled RNA polymerase II transcription bubbles (7). However, the detection and signaling of CPT-induced, transcription-dependent DNA damage are not well understood, nor is it clear

* This work was supported, in whole or in part, by National Institutes of Health Grant CA124722. This work was also supported by a grant from the American Cancer Society, a Shaw Scientist Award (to R. S. T.) from the Greater Milwaukee Foundation, and by Grant-in-aid 20659047 from Japan Society for the Promotion of Science for Exploratory Research (to H. T.).

[S] The on-line version of this article (available at http://www.jbc.org) contains supplemental Figs. S1–S5.

[1] To whom correspondence should be addressed: Dept. of Molecular Oncology, Graduate School of Medical Sciences, Kyushu University, Fukuoka 812-8582, Japan. E-mail: sakasai@surg2.med.kyushu-u.ac.jp.

[2] The abbreviations used are: TopI, topoisomerase I; TopI-cc, TopI cleavage complex; CPT, camptothecin; DSB, double-strand break; DSE, double-strand end; DNA-PK, DNA-dependent protein kinase; HR, homologous recombination; ATM, ataxia telangiectasia mutated; ATR, ATM and Rad3-related; DRB, 5,6-dichloro-1-β-D-ribofuranosylbenzimidazole; HU, hydroxyurea; siRNA, small interfering RNA; BrdUrd, bromodeoxyuridine; IR, ionizing radiation; 53BP1, p53-binding protein 1; RPA2, replication protein A2.

whether transcription-mediated DNA damage contributes significantly to CPT cytotoxicity.

In this study, we investigated transcription-dependent and -independent pathways activated by CPT in human cells. We show that ATM is critically important for initiation of the G_1/S phase checkpoint in response to CPT and that transcription-dependent activation of ATM in G_1 phase suppresses DNA strand breakage leading to DNA-PK activation in S phase cells. These findings have implications for understanding CPT tumoricidal activity.

EXPERIMENTAL PROCEDURES

Cell Culture and Irradiation—HeLa, U2OS, and HCT116 cells were obtained from American Type Culture Collection and maintained in Dulbecco's modified Eagle's medium with 10% fetal bovine serum. SV40-transformed GM00637H (ATM+), GM05849C (ATM−), (obtained from Coriell Cell Repositories), and hTERT-immortalized SuSa/Tn (ATM+), AT1OS/Tn (ATM−) (kindly provided by Dr. K Ishizaki) (8) were cultured in Dulbecco's modified Eagle's medium with 10% fetal bovine serum. Cells were UV- and IR-irradiated as reported (9). CPT, VP-16, 5,6-dichloro-1-β-D-ribofuranosylbenzimidazole (DRB), KU-55933, NU7026, hydroxyurea (HU), and thymidine were purchased from Sigma. To knock down TopBP1 and RNF8 expression, siRNA SMART pool targeting each gene (Dharmacon) was used. siRNAs were transfected as described (10).

Antibodies and Immunofluorescence—Antibodies were obtained from following suppliers: Bethyl Laboratories (p53-binding protein 1 (53BP1), A300-272A), Oncogene (replication protein A (RPA), Ab-3; BrdUrd, Ab-2), Millipore (γH2AX, JBW301), Calbiochem (Rad51, PC130), Abcam (phospho-DNA-PKcs, ab18192, Chk2, ab8108), R&D Systems (phospho-ATM, AF-165; phospho-Chk1 Ser^{317}, AF-2054; phospho-Chk2, AF-1626), GeneTex (ATM, GTX70103), Thermo Scientific (DNA-PKcs, Ab-4), Cell Signaling Technology (phospho-Chk1 S345, no.2341), and Santa Cruz Biotechnology (Chk1, G-4). Cell preparation for staining of 53BP1, γH2AX and incorporated BrdUrd was performed as described (9). For RPA2 and Rad51 staining, cells were preextracted with phosphate-buffered saline containing 0.1% Triton X-100. The fixed cells were incubated with primary antibodies specific for 53BP1, BrdUrd, γH2AX, and Rad51. After incubation with secondary antibodies, cell nuclei were stained with 4′,6-diamidino-2-phenylindole (2 μg/ml). A Carl Zeiss Axiovert 200 fluorescence microscope or LSM510 laser-scanning microscope was used to visualize samples.

Western Blotting—Cell lysis, SDS-PAGE, and gel transfer were performed as described (9). After incubation with secondary antibody, the membranes were visualized using SuperSignal chemiluminescent substrate (Pierce).

Cell Cycle Synchronization and Flow Cytometry—To synchronize cells in the S phase, cells were treated with thymidine at 2.5 mM for 18 h and incubated with a fresh medium for 5 h. To collect G_1 phase cells, cells were treated with nocodazole for 12 h and released with a fresh medium for 5 h. For cell cycle analysis, cells were harvested and stained with propidium iodide after fixing with 70% ethanol. Propidium iodide-stained cells were analyzed using a FACSCalibur (BD Biosciences).

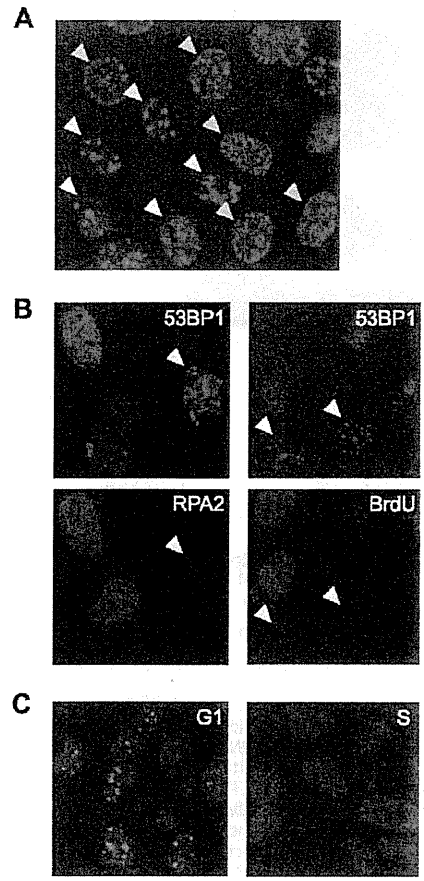

FIGURE 1. **CPT induces two distinct types of 53BP1 foci.** *A*, representative image of 53BP1 foci induced by CPT (2 μM, 1 h) treatment. The HeLa cells denoted by *white arrowheads* represent Type I 53BP1 foci, whereas *yellow arrowheads* denote Type II foci. *B*, Type I 53BP1 foci occurring in non-S phase cells. HeLa cells were treated with CPT (2 μM, 1 h) and stained with anti-53BP1 and RPA2 antibodies (*left*). To observe DNA synthesis, cells were treated with BrdUrd (20 μM, 20 min) and stained with α-53BP1 and α-BrdUrd antibodies (*right*). C, CPT-induced 53BP1 foci in G_1 or S phase cells. Cells were synchronized in G_1 phase and S phase by release from nocodazole block and thymidine block, respectively. After treatment with CPT (2 μM, 1 h), cells were stained with anti-53BP1 antibody.

Neutral Comet Assay—Cells were suspended in 0.7% low melting point agarose and spread on glass slides precoated with 1% agarose. Slides were overlaid with coverslips that were removed after the gel solidified. The gel was treated with lysis solution (Trevigen) for 30 min at 4 °C in the dark and electrophoresed at 1 V/cm for 17 min. Comet tails were stained with SYBR Green I (BMA) and analyzed by fluorescent microscope.

RESULTS

CPT Induces Two Types of 53BP1 Foci in Mammalian Cells—53BP1 is an adaptor protein that is recruited to nuclear foci in response to genotoxic stimuli, including ionizing radiation-induced DSBs and CPT-associated DSEs (11, 12). Following the treatment of HeLa cells with CPT, we observed two distinct 53BP1 localization patterns: Type I exhibited large 53BP1 foci that typically numbered fewer than 15/cell; Type II displayed

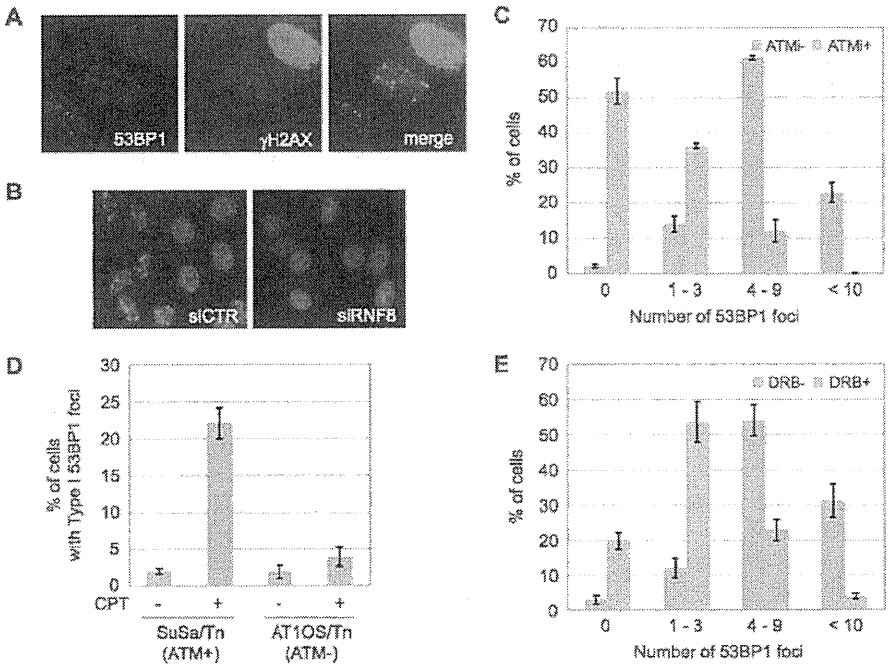

FIGURE 2. **Type I 53BP1 foci are ATM-dependent and occur in response to transcription-mediated DNA damage.** *A*, co-staining 53BP1 with γH2AX. HeLa cells were treated with CPT (2 μM, 1 h) and stained with α-53BP1 and γH2AX antibodies. *B*, formation of 53BP1 foci requiring RNF8. HeLa cells were transfected with nontargeting (*siCTR*) or RNF8-targeting siRNA (*siRNF8*) and stained with anti-53BP1 antibody following CPT (2 μM, 1 h) treatment. *C*, effect of ATM inhibition on Type I 53BP1 foci formation. HeLa cells were treated with solvent only, KU-55933 (10 μM, 1 h) before CPT (2 μM, 1 h) treatment, and stained with anti-53BP1 and anti-RPA2 antibodies. *D*, Type I 53BP1 foci in ATM-deficient cells. Control cells (*SuSa/Tn*) and ATM-deficient cells (*AT1OS/Tn*) were treated with CPT (2 μM, 1 h) and stained with anti-53BP1 and anti-RPA2 antibodies. *E*, effect of transcription inhibition on Type I 53BP1 foci formation. HeLa cells were treated with DRB (100 μM, 2 h) before CPT (2 μM, 1 h) treatment and stained with anti-53BP1 and anti-RPA2 antibodies. The number of 53BP1 foci observed in cells without RPA2 signal was counted. *Error bars* show S.E. calculated from three independent experiments.

many smaller foci (Fig. 1*A*). To characterize Type I and Type II foci further, we co-stained the cells with antibodies specific for the 32-kDa subunit of replication protein A (RPA2) following cellular preextraction with detergent. The presence of detergent-resistant RPA2 foci was used to distinguish S phase cells from G_1 phase cells (13). We found that cells possessing Type I 53BP1 foci were not co-stained for RPA2, whereas cells possessing Type II 53BP1 foci were (Fig. 1*B*). This finding suggested that Type I 53BP1 foci are formed predominantly in non-S phase cells. Consistent with this idea, cells displaying Type I 53BP1 foci did not incorporate BrdUrd, supporting the assertion that they are in either in G_1 or G_2/M phase (Fig. 1*B*). To substantiate this finding further, we used cell cycle synchronization to show that G_1 phase cells treated with CPT displayed Type I 53BP1 foci, whereas Type II 53BP1 foci were predominantly observed in S phase cells following CPT treatment (Fig. 1*C*). These results raised the possibility that Type I, DNA replication-independent, 53BP1 foci are caused by transcription-mediated DNA damage.

Formation of Type I 53BP1 Foci Requires RNF8, ATM, and Active Transcription—To characterize the CPT-induced Type I 53BP1 foci further, we examined co-localization of 53BP1 with a well established marker of DNA damage, phosphorylated-H2AX (γH2AX). We found that Type I foci were co-localized with γH2AX. On the other hand, γH2AX showed an intense, pan-nuclear signal in cells displaying Type II 53BP1 foci (Fig. 2*A*). The E3 ubiquitin ligase RNF8 is required for 53BP1 foci formation in response to DSBs induced by IR (14–16), and we found that RNF8 knockdown also sharply suppressed CPT-induced 53BP1 foci (Fig. 2*B* and supplemental Fig. S1). To test for the dependence of this response on ATM, HeLa cells were treated with the ATM inhibitor KU-55933 coincident with CPT treatment and co-stained with 53BP1 and RPA2. Focusing solely on RPA2-negative, non-S phase cells, we found that the number of Type I 53BP1 foci/cell was suppressed in KU-55933-treated cells as well as ATM-deficient cells (Fig. 2, *C* and *D*). These findings strongly suggested that Type I 53BP1 foci were formed in an ATM-dependent manner.

CPT interferes with RNA transcription, and transcription-associated DNA damage linked to ATM activation has recently been reported (7). Therefore, we tested the transcription dependence of CPT-induced 53BP1 foci by treating cells with DRB, a CDK inhibitor, that suppresses the phosphorylation of polymerase II C-terminal domain required for transcription elongation (17–19). Cells pretreated with DRB showed a drastic reduction in Type I 53BP1 foci (Fig. 2*E*). Taken together, these data demonstrate that, in non-S phase cells, CPT causes transcription-mediated DNA damage leading to the ATM and RNF8-dependent accumulation of 53BP1 foci.

Transcription-dependent ATM Activation in Response to CPT—The above experiments using DRB suggested that CPT-induced ATM activation is dependent on transcription. However, DNA replication-mediated DSEs are thought to account for the majority of CPT-induced DNA damage. To assess the relative contributions of transcription-associated *versus* replication-associated DNA damage to the activation of downstream pathways, HeLa cells were pretreated with inhibitors of DNA replication and transcription prior to the addition of CPT. Treatment with the replication inhibitor HU for 10 min effectively suppressed DNA synthesis (supplemental Fig. S2) and virtually abolished CPT-induced RPA2 phosphorylation (Fig. 3, *left*). Thymidine treatment prior to CPT addition also suppressed RPA2 phosphorylation (Fig. 3, *left*), indicating that RPA2 phosphorylation is highly dependent on DNA replication. In contrast, neither CPT-induced ATM autophosphorylation on Ser^{1981} nor ATM-dependent phosphorylation of Chk2 on Thr^{68} was suppressed by DNA replication inhibition

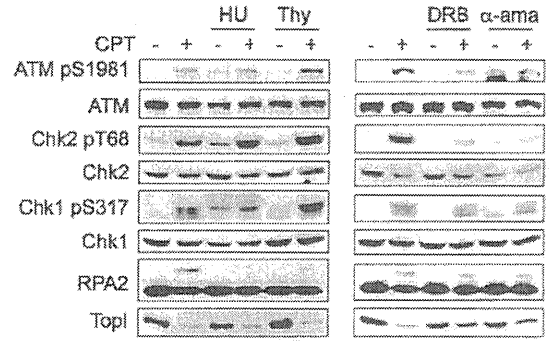

FIGURE 3. **Transcription-dependent ATM activation in response to CPT.** HeLa cells were pretreated with DNA replication inhibitors (HU and thymidine (Thy), 2 mM and 2.5 mM, respectively) or transcription inhibitors (DRB and α-amanitin, 100 μM and 5 μM, respectively) before CPT (2 μM, 1 h) treatment. DNA damage signaling was analyzed by Western blotting using appropriate antibodies.

(Fig. 3, *left*). These results imply that CPT-dependent activation of ATM does not absolutely require DNA replication.

In stark contrast to results using DNA replication inhibitors, the transcriptional inhibitors DRB and α-amanitin apparently suppressed CPT-induced ATM autophosphorylation at Ser^{1981} and Chk2 phosphorylation on Thr^{68} (Fig. 3, *right*). These results are consistent with previous reports demonstrating that CPT-induced ATM activation is dependent on transcription in non-cycling cells (7, 20). Our data further indicate that transcription-coupled events account for the bulk of ATM activation by CPT, even in actively dividing cells. Importantly, the transcription dependence of ATM activation established with CPT was not observed with other DNA-damaging agents, such as IR, the topoisomerase II inhibitor VP-16, and UV light (supplemental Fig. S3). These findings indicate that TopI poisons uniquely induce transcription-coupled DNA damage that signals to ATM.

ATM Is Required for CPT-induced Checkpoint Responses—To examine a possibility that ATM contributes to CPT-induced cell cycle checkpoint regulation, U2OS cells were treated with the ATM inhibitor KU-55933, exposed to CPT, and then monitored in cell cycle distribution by flow cytometry. Whereas U2OS cells treated with dimethyl sulfoxide or the DNA-PK inhibitor NU7026 exhibited prolonged G_1 arrest up to 12 h following CPT treatment, U2OS cells treated with KU-55933 began exiting G_1 phase by 6 h (Fig. 4*A*). This indicates that CPT induces an ATM-dependent G_1/S checkpoint. Consistent with a defect in the G_1/S phase checkpoint, ATM-inhibited U2OS cells rapidly accumulated in the S phase between 6 and 12 h after CPT treatment (Fig. 4*B*). By 24 h after CPT exposure, however, ATM-inhibited cells exited S phase and accumulated in the G_2 phase, which is indicative of a defect in S phase checkpoint maintenance (Fig. 4*B* and supplemental Fig. S4). In contrast, inhibition of DNA-PK did not result in S phase accumulation of U2OS cells at early time points (6–12 h), nor did the inhibitor cause premature S phase checkpoint release (Fig. 4*B*). Together, these results suggest that ATM, but not DNA-PK, is involved in CPT-induced G_1/S and S phase checkpoint activation.

Based on the ATM contribution to S phase checkpoint activation, we further analyzed the effect of ATM on the ATR-Chk1 pathway. Autophosphorylation of ATM Ser^{1981} and DNA-PKcs Ser^{2056} was used to monitor ATM and DNA-PK activation, respectively, whereas Chk1 Ser^{317} phosphorylation was used as a surrogate marker for ATR activation. Treatment with caffeine (2 mM) had no effect on ATM and DNA-PKcs autophosphorylation, but strongly suppressed Chk1 phosphorylation (supplemental Fig. S5), which is consistent with the previous finding that ATR is the primary Chk1-activating kinase in response to TopI poisons (4). ATM inhibition also strongly suppressed Chk1 phosphorylation, indicating that both ATM and ATR are required for full Chk1 activation in response to CPT (supplemental Fig. S5).

To analyze CPT-induced Chk1 phosphorylation further, we performed knockdown of TopBP1, a direct activator of ATR that is required for Chk1 phosphorylation in response to IR, UV, and HU (21). HeLa cells were transfected with siRNA against TopBP1, and the phosphorylation of Chk1, Chk2, and RPA2 was analyzed by Western blotting. CPT-induced Chk1 phosphorylation was suppressed in TopBP1 knockdown cells, whereas Chk2 phosphorylation was not (Fig. 4*C*), implying that CPT-induced Chk1 phosphorylation requires TopBP1 and suggesting that ATM is upstream of TopBP1 in the pathway leading to Chk1 phosphorylation. RPA2 phosphorylation was not suppressed by TopBP1 knockdown (Fig. 4*C*). Given that CPT-induced phosphorylation of RPA2 is reported to be ATR-dependent (22), this finding indicates that ATR can be activated independent of TopBP1 in CPT-treated cells. Finally, we used synchronized HeLa cells to show that CPT-induced TopBP1 and Chk1 phosphorylation are restricted to S phase cells and are dependent on ATM (Fig. 4*D*). From these findings, we propose the existence of an ATM-TopBP1-ATR-Chk1 signaling pathway that is activated by CPT in S phase cells. Because transcription inhibition only slightly affected CPT-induced Chk1 phosphorylation, replication-coupled DSEs, but not transcription-coupled DNA damage, probably trigger this pathway.

Hyperactivation of DNA-PK in ATM-inhibited Cells—The above findings are consistent with a model in which CPT caused the transcription-coupled activation of an ATM-dependent G_1/S checkpoint. Interestingly, we found that CPT-induced activation of DNA-PK was strongly potentiated when ATM was inhibited in HeLa cells (Fig. 5*A*). This result was also observed in ATM-deficient cells (Fig. 5*B*). The enhanced DNA-PKcs autophosphorylation observed in the presence of the ATM inhibitor KU-55933 was suppressed by HU treatment, indicating that DNA-PK hyperactivation by ATM inhibition requires ongoing DNA replication (Fig. 5*A*). This finding is consistent with our earlier report that CPT-induced DNA-PK activation is strongly dependent on DNA replication (23). DRB also partially inhibited CPT-induced DNA-PK autophosphorylation, which is consistent with the notion that transcription-coupled events lie upstream of DNA-PK activation (Fig. 5*A*).

A plausible explanation for the DNA replication and transcription-dependent hyperactivation of DNA-PK in ATM-inhibited cells is that ATM inhibition led to the defect in G_1/S and S phase checkpoints and the carryover of transcription-mediated strand breaks into the S phase, where such lesions were converted to frank DSEs activating DNA-PK. To test this possibility, we used neutral comet assays to assess CPT-induced

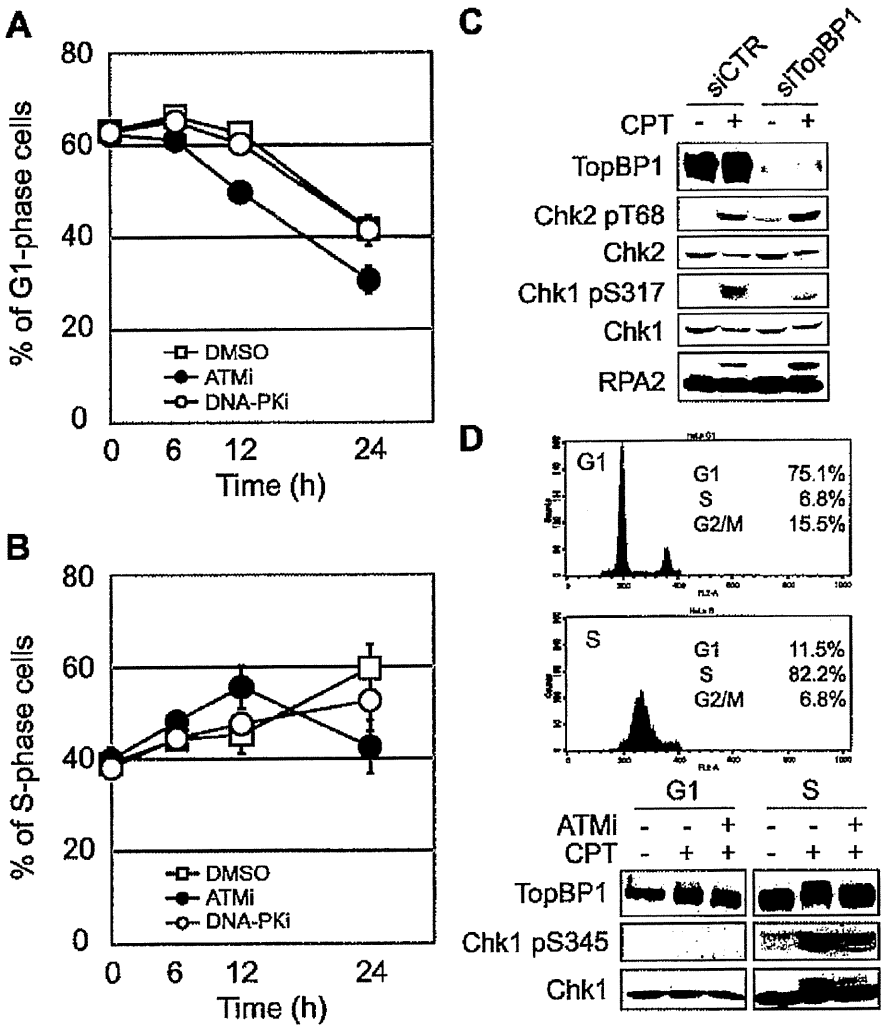

FIGURE 4. **CPT induces ATM-dependent G_1/S and S phase checkpoint arrest.** *A* and *B*, U2OS cells were treated with 1 μM CPT following treatment with ATM (KU-55933; 10 μM, 1 h) or DNA-PK inhibitor (NU7026; 10 μM, 1 h). After incubation for the indicated time, cells were fixed with ethanol for propidium iodide staining. Cell cycle distribution was analyzed by flow cytometry, and the percentage of cells in G_1 phase and S phase was plotted in *A* and *B*, respectively. *Error bars* show S.E. calculated from three independent experiments. *C*, CPT-induced Chk1 phosphorylation is TopBP1-dependent. HeLa cells transfected with control (*siCTR*) or TopBP1 siRNA (*siTopBP1*) were treated with CPT (2 μM, 1 h), and then Chk2, Chk1, and RPA2 phosphorylation were analyzed by Western blotting with the indicated antibodies. *D*, CPT-induced TopBP1 phosphorylation is restricted to S phase. To synchronize cell cycle in the G_1 and S phase, HeLa cells were released from nocodazole block and thymidine block, respectively. Both cell populations were treated with CPT (2 μM, 1 h) with or without ATM inhibitor (KU-55933; 10 μM, 1 h). TopBP1, Chk1, and Chk1 phosphorylation was detected by Western blotting using the indicated antibodies.

DSEs in cells treated with ATM inhibitor or vehicle. As expected, CPT treatment caused an increase in comet tail moment, reflecting the generation of DNA strand breaks (Fig. 5*C*). Cells co-treated with CPT and the ATM inhibitor demonstrated an ~2.5-fold increase in comet tail moment compared with cells treated with CPT alone, supporting the contention that accumulation of DSEs is responsible for DNA-PK hyperactivation in the absence of functional ATM. Finally, as predicted based on the DNA-PK autophosphorylation results, the accumulation of DNA strand breaks in CPT and ATM inhibitor-treated cells was reduced by DRB treatment (Fig. 5*C*). These results are consistent with a model whereby transcription-mediated strand breaks are carried over from G_1 phase to S phase in ATM-inhibited cells, where they are converted into DSEs upon collision with DNA replication forks.

Substantiation of the above model required us to test whether CPT-induced transcription-mediated strand breaks arising in the G_1 phase are in fact responsible for DNA-PK hyperactivation. To test this possibility, U2OS cells were synchronized in the G_1 phase as schematically indicated in Fig. 5*D*. G_1-synchronized cells were incubated with KU-55933 for 1 h prior to CPT exposure. CPT treatment was performed only for 1 h during G_1 phase to avoid the possibility of direct DSE generation in S phase. At 0 h, 1 h, and 5 h after CPT addition, DNA-PKcs autophosphorylation was analyzed by Western blotting. There was no significant difference in S phase percentages between untreated and ATM inhibitor-treated cells in the absence of CPT, indicating that ATM inhibition does not affect S phase entry in this system (Fig. 5*D*). We found that CPT-induced DNA-PKcs autophosphorylation was enhanced in cells treated with the ATM inhibitor in the G_1 phase *versus* cells treated with CPT alone (Fig. 5*D*). Overall, the findings demonstrate that ATM activates a G_1/S checkpoint in response to CPT-mediated transcriptional collapse. Failure of this checkpoint leads to the carryover of transcription-mediated strand breaks into the S phase, resulting in DSE generation and hyperactivation of DNA-PK.

DNA-PK Promotes CPT-induced Cell Death in the Absence of ATM—Given that inhibition of ATM led to DNA-PK hyperactivation in CPT-treated cells, we reasoned that dual inhibition of ATM and DNA-PK would lead to synergistic cell killing by CPT. To address this possibility, the effect of ATM or/and DNA-PK inhibition on CPT-sensitivity was analyzed in HCT116 colon carcinoma cells. In HCT116 cells, we found that ATM inhibition caused moderate CPT hypersensitivity, whereas DNA-PK inhibition actually led to a small, yet reproducible, increase in HCT116 cell survival following CPT treatment (Fig. 6*A*). This result is consistent with previous findings showing that DNA ligase IV- or Ku70-deficient chicken DT40 cells display partial CPT resistance (24, 25). Interestingly, we found that DNA-PK inhibition rescued the CPT-hypersensitive phenotype of ATM-

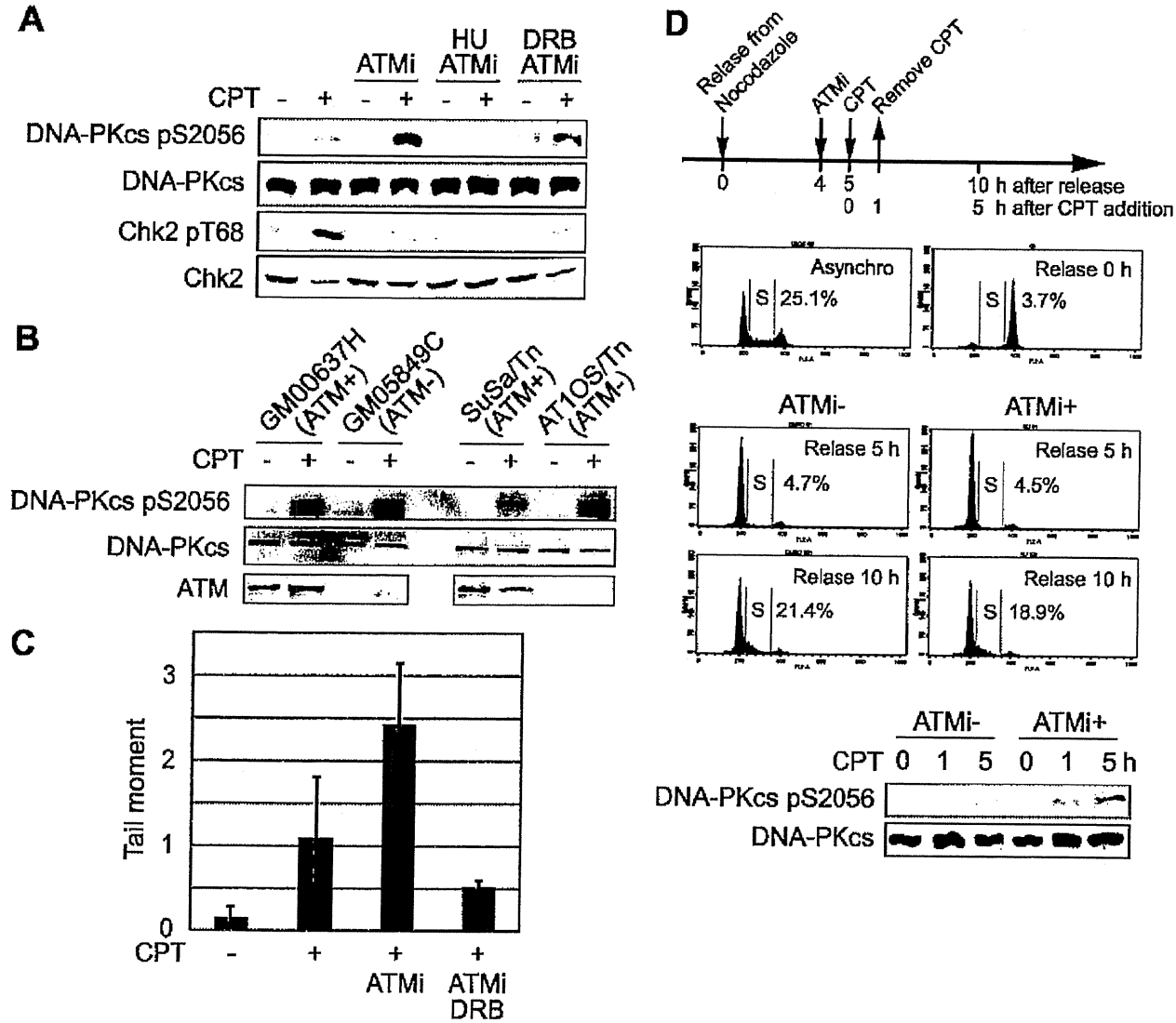

FIGURE 5. **ATM suppresses DNA-PK activation in response to CPT.** *A*, effects of ATM, replication, and transcription inhibitors on CPT-induced DNA-PKcs autophosphorylation. HeLa cells were treated with CPT (2 μM, 1 h) following ATM inhibitor (KU-55933; 10 μM, 1 h) with HU (2 mM, 10 min) or DRB (100 μM, 2 h) treatment, and DNA-PKcs autophosphorylation and Chk2 phosphorylation were analyzed by Western blotting. *B*, DNA-PK activation in ATM-deficient cells. Control cells (GM00637H or SuSa/Tn) and ATM-deficient cells (GM05849C or AT1OS/Tn) were treated with CPT (2 μM, 1 h), and DNA-PKcs autophosphorylation were analyzed by Western blotting. *C*, comet assay for detection of CPT-induced DNA strand breaks. HeLa cells were treated with CPT (0.25 μM) for 1 h following ATM inhibitor (10 μM, 1 h) treatment in the absence or presence of DRB (100 μM, 2 h), and induced-DNA strand breaks were detected by neutral comet assay. The comet tail moments were averaged in triplicate experiments, where the median among 100 cells was calculated in each experiment. *Error bars* represent S.E. calculated from three independent experiments. *D*, inhibition of ATM leads to DNA damage carry over from G_1 to S phase. U2OS cells were synchronized in M phase with nocodazole and released into G_1 and S phase upon incubation with fresh medium. Flow cytometry histograms show cell cycle profiles after release from the nocodazole block in the absence or presence of KU-55933 (10 μM, 1 h). Where indicated, cells were treated with CPT (5 μM, 1 h). The status of DNA-PK activation in the different experimental samples was determined by Western blotting with anti-phospho-DNA-PK antibodies.

inhibited cells (Fig. 6*A*). At a low dose (5 nM) of CPT, HCT116 cells exposed to both DNA-PK and ATM inhibitors showed a 10-fold increase in colony formation *versus* HCT116 cells cultured only in the presence of the ATM inhibitor. This finding suggested that cytotoxicity of CPT is associated with DNA-PK activation.

Given that CPT-induced DSEs are repaired predominantly through HR-dependent pathways in the S phase (2), we reasoned that hypersensitivity of ATM-inhibited cells might be linked to defective HR repair. To test this idea, we measured the formation of Rad51 foci, a surrogate marker for HR, in HeLa cells exposed to CPT in the presence of ATM and DNA-PK inhibitors. CPT treatment for 6 h increased the percentage of cells displaying Rad51 foci from 4% to 11% (Fig. 6*B*). Co-exposure of cells to KU-55933 attenuated CPT-induced Rad51 foci formation, suggesting that ATM contributes to HR repair of these lesions. Surprisingly, the DNA-PK inhibitor treatment also suppressed the percentage of cells with Rad51 foci, and the combination of ATM and DNA-PK inhibition further reduced the percentage of Rad51 foci-positive cells. These findings imply that DNA-PK and ATM cooperatively contribute to the HR pathway in response to CPT and that phe-

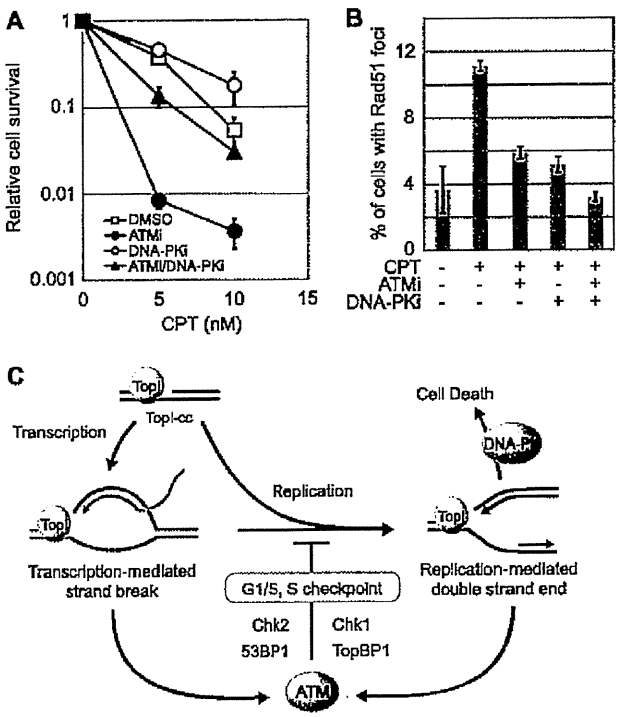

FIGURE 6. **DNA-PK activation promotes cells death in response to CPT.** *A*, clonogenic survival assays of HCT-116 cells treated with CPT in the absence or presence of ATM and/or DNA-PK inhibitors. Cells pretreated with ATM inhibitor (KU-55933; 10 μM, 1 h) and/or DNA-PK inhibitor (NU7026; 10 μM, 1 h) were cultured in the presence of CPT for 2 days at the indicated concentration. *Error bars* show S.E. calculated from three independent experiments. *B*, effects of ATM and/or DNA-PK inhibition on Rad51 foci formation. HeLa cells were treated with CPT (2 μM, 6 h) following pretreatment with ATM (10 μM, 1 h) and/or DNA-PK (10 μM, 1 h) inhibitors, and then cells were stained with anti-Rad51 antibody. The cells with over 10 foci were considered Rad51 foci-positive, and the percentage of Rad51 foci-positive cells is depicted graphically. *Error bars* show S.E. calculated from three independent experiments. *C*, schematic model summarizing the CPT-induced cellular responses. Transcription-mediated strand breaks caused by CPT in G_1 phase are converted to double strand end by DNA replication. ATM is activated against both DNA damages and induces G_1/S and S phase checkpoints to prevent DNA-PK hyperactivation leading to cell death.

notypic rescue of CPT hypersensitivity in cells co-treated with ATM and DNA-PK inhibitors is unlikely due to restoration of HR repair.

DISCUSSION

In this study we have explored the complex mechanisms of signal transduction following exposure of cancer cell lines to a TopI poison, CPT. The most salient findings in the study include: (i) CPT induces transcription-dependent and -independent activation of ATM leading to 53BP1 foci formation and checkpoint activation; (ii) the absence of ATM-dependent G_1/S checkpoint leads to severe DNA damage and DNA-PK hyperactivation in the S phase; (iii) hyperactivation of DNA-PK by CPT in the absence of ATM causes cell death. Taken together, the present findings illuminate important details of the cellular response to a clinically relevant class of chemotherapeutics.

The mechanism of DNA strand breakage induced by CPT and clinically useful derivatives, irinotecan and topotecan, has been the subject of intensive study, and it is well established that TopI-cc are converted to frank DSBs during S phase (1). Transcription-mediated strand breaks are thought to be structurally distinct from DSBs caused by other DNA-damaging agents, such as IR or bleomycin. Because transcription bubbles comprised unwound DNA and nascently synthesized RNA, it is possible that transcription-mediated strand breaks contain a DNA·RNA hybrid end. Consistent with this hypothesis, CPT-induced DNA-PK activation is markedly dependent on DNA replication and was very weak in cells synchronized in G_1 phase. In 1986, Mimori and Hardin (26) reported reduced affinity of the Ku heterodimer for DNA·RNA hybrid probes compared with DNA·DNA double-strand probes. The strong preference of Ku/DNA-PK complexes for double strand DNA *versus* DNA·RNA hybrids plausibly explains why DNA-PK is not activated by CPT in G_1 phase cells. On the other hand, the transcription-dependent activation of ATM, which has been reported here and recently reported by Sordet *et al.* (7), implies that ATM can be activated by DNA·RNA hybrids, although the precise mechanism is not known.

Our results suggested that one end result of transcription-dependent ATM activation is the induction of Chk2 phosphorylation and G_1/S checkpoint arrest. ATM also clearly participates in S phase checkpoint signaling in response to CPT. In S phase cells, ATM promoted TopBP1 phosphorylation and TopBP1-dependent Chk1 activation. The finding implies that ATM and ATR function in a linear pathway, as has been proposed for IR-induced responses (27). Interestingly, CPT-induced RPA2 phosphorylation was not TopBP1-dependent in our hands. Given that ATR is involved in RPA2 phosphorylation (22, 28), this finding implies that TopBP1 is required for only a subset of ATR-dependent phosphorylation events. To summarize these findings, we found that ATM is critical for both G_1 and intra-S phase arrest in response to CPT, which activates two independent ATM activation pathways: a transcription-dependent pathway that is active in the G_1 phase and signals through Chk2, and a DNA replication-dependent pathway that is active in the S phase and signals through TopBP1 and Chk1 (Fig. 6*C*).

In the absence of an ATM-dependent G_1/S checkpoint, transcription-mediated strand breaks caused by CPT are carried over into the S phase, where they are converted into frank DSBs, presumably as a consequence of collisions between stalled transcription complexes and DNA replication forks. As a result, DNA-PK is hyperactivated. In HCT116 cells, the hyperactivation of DNA-PK in the absence of functional ATM leads to a dramatic loss of colony-forming activity. In addition, treatment with only the DNA-PK inhibitor imparted moderate CPT resistance to HCT116 cells, indicating that DNA-PK influences cell survival independent of ATM status. The rescue of CPT sensitivity in ATM-inhibited cells by DNA-PK inhibition cannot be explained by enhanced HR repair because Rad51 foci formation was not promoted by DNA-PK inhibition. Adachi *et al.* (24) have reported similar results showing that DNA ligase IV deletion rescued CPT sensitivity of Rad54-deficient chicken DT40 cells. Although the mechanistic basis for DNA-PK-dependent loss of viability in CPT-treated cells is not clear, we envision two nonexclusive models: first, activation of DNA-PK

could lead to deleterious nonhomologous end joining, which antagonizes survival by promoting deleterious DNA end-joining reactions that preclude HR (24); second, DNA-PK harbors an intrinsic proapoptotic function that is triggered by replication-mediated DSEs. The participation of DNA-PK in apoptosis is complex, with the reports showing prosurvival and proapoptosis functions (29–32). Thus, in the absence of ATM, it is possible that CPT activates a latent, proapoptotic function of DNA-PK. Viewing from a different perspective, our findings raise a question as to how ATM antagonizes DNA-PK-dependent apoptosis in CPT-treated cells. The simplest explanation is that ATM prevents the accumulation of catastrophic S phase damage required to activate DNA-PK. However, it is possible that a more direct antagonism between ATM and DNA-PK exists, at the level of undefined substrate phosphorylation.

In summary, we have shown that ATM responds to CPT-caused transcription collapse and activates cell cycle checkpoints with subsequent prevention of DSE generation and DNA-PK-mediated cell death. These findings indicate that DNA-PK functional status may be an important predictor of CPT treatment efficacy and that pharmacologic abrogation of the G_1/S checkpoint should enhance CPT sensitivity of tumors. These findings provide rationale for further development and preclinical testing of ATM inhibitors and other G_1/S checkpoint modifiers as adjuvants to TopI poison-based therapies.

REFERENCES

1. Pommier, Y. (2006) *Nat. Rev. Cancer* **6**, 789–802
2. Arnaudeau, C., Lundin, C., and Helleday, T. (2001) *J. Mol. Biol.* **307**, 1235–1245
3. Klein, H. L., and Kreuzer, K. N. (2002) *Mol. Cell* **9**, 471–480
4. Cliby, W. A., Lewis, K. A., Lilly, K. K., and Kaufmann, S. H. (2002) *J. Biol. Chem.* **277**, 1599–1606
5. Wang, J. L., Wang, X., Wang, H., Iliakis, G., and Wang, Y. (2002) *Cell Cycle* **1**, 267–272
6. Wu, J., and Liu, L. F. (1997) *Nucleic Acids Res.* **25**, 4181–4186
7. Sordet, O., Redon, C. E., Guirouilh-Barbat, J., Smith, S., Solier, S., Douarre, C., Conti, C., Nakamura, A. J., Das, B. B., Nicolas, E., Kohn, K. W., Bonner, W. M., and Pommier, Y. (2009) *EMBO Rep.* **10**, 887–893
8. Nakamura, H., Fukami, H., Hayashi, Y., Kiyono, T., Nakatsugawa, S., Hamaguchi, M., and Ishizaki, K. (2002) *J. Radiat. Res.* **43**, 167–174
9. Sakasai, R., and Tibbetts, R. (2008) *J. Biol. Chem.* **283**, 13549–13555
10. Dodson, G. E., and Tibbetts, R. S. (2006) *J. Biol. Chem.* **281**, 1692–1697
11. Wang, B., Matsuoka, S., Carpenter, P. B., and Elledge, S. J. (2002) *Science* **298**, 1435–1438
12. Rappold, I., Iwabuchi, K., Date, T., and Chen, J. (2001) *J. Cell Biol.* **153**, 613–620
13. Dimitrova, D. S., and Gilbert, D. M. (2000) *Exp. Cell Res.* **254**, 321–327
14. Mailand, N., Bekker-Jensen, S., Faustrup, H., Melander, F., Bartek, J., Lukas, C., and Lukas, J. (2007) *Cell* **131**, 887–900
15. Kolas, N. K., Chapman, J. R., Nakada, S., Ylanko, J., Chahwan, R., Sweeney, F. D., Panier, S., Mendez, M., Wildenhain, J., Thomson, T. M., Pelletier, L., Jackson, S. P., and Durocher, D. (2007) *Science* **318**, 1637–1640
16. Huen, M. S., Grant, R., Manke, I., Minn, K., Yu, X., Yaffe, M. B., and Chen, J. (2007) *Cell* **131**, 901–914
17. Sehgal, P. B., Derman, E., Molloy, G. R., Tamm, I., and Darnell, J. E. (1976) *Science* **194**, 431–433
18. Peng, J., Zhu, Y., Milton, J. T., and Price, D. H. (1998) *Genes Dev.* **12**, 755–762
19. Dubois, M. F., Bellier, S., Seo, S. J., and Bensaude, O. (1994) *J. Cell. Physiol.* **158**, 417–426
20. Lin, C. P., Ban, Y., Lyu, Y. L., Desai, S. D., and Liu, L. F. (2008) *J. Biol. Chem.* **283**, 21074–21083
21. Liu, S., Bekker-Jensen, S., Mailand, N., Lukas, C., Bartek, J., and Lukas, J. (2006) *Mol. Cell. Biol.* **26**, 6056–6064
22. Sakasai, R., Shinohe, K., Ichijima, Y., Okita, N., Shibata, A., Asahina, K., and Teraoka, H. (2006) *Genes Cells* **11**, 237–246
23. Sakasai, R., Teraoka, H., and Tibbetts, R. S. (2010) *DNA Repair* **9**, 76–82
24. Adachi, N., So, S., and Koyama, H. (2004) *J. Biol. Chem.* **279**, 37343–37348
25. Hochegger, H., Dejsuphong, D., Fukushima, T., Morrison, C., Sonoda, E., Schreiber, V., Zhao, G. Y., Saberi, A., Masutani, M., Adachi, N., Koyama, H., de Murcia, G., and Takeda, S. (2006) *EMBO J.* **25**, 1305–1314
26. Mimori, T., and Hardin, J. A. (1986) *J. Biol. Chem.* **261**, 10375–10379
27. Yoo, H. Y., Kumagai, A., Shevchenko, A., Shevchenko, A., and Dunphy, W. G. (2007) *J. Biol. Chem.* **282**, 17501–17506
28. Anantha, R. W., Vassin, V. M., and Borowiec, J. A. (2007) *J. Biol. Chem.* **282**, 35910–35923
29. Bozulic, L., Surucu, B., Hynx, D., and Hemmings, B. A. (2008) *Mol. Cell* **30**, 203–213
30. Gurley, K. E., Moser, R., Gu, Y., Hasty, P., and Kemp, C. J. (2009) *EMBO Rep.* **10**, 87–93
31. Cobb, L. J., Liu, B., Lee, K. W., and Cohen, P. (2006) *Cancer Res.* **66**, 10878–10884
32. Callén, E., Jankovic, M., Wong, N., Zha, S., Chen, H. T., Difilippantonio, S., Di Virgilio, M., Heidkamp, G., Alt, F. W., Nussenzweig, A., and Nussenzweig, M. (2009) *Mol. Cell* **34**, 285–297

JVI
Journals ASM.org

Production of Infectious Chimeric Hepatitis C Virus Genotype 2b Harboring Minimal Regions of JFH-1

Asako Murayama,[a] Takanobu Kato,[a] Daisuke Akazawa,[a] Nao Sugiyama,[a] Tomoko Date,[a] Takahiro Masaki,[a] Shingo Nakamoto,[b] Yasuhito Tanaka,[c] Masashi Mizokami,[d] Osamu Yokosuka,[b] Akio Nomoto,[e]* and Takaji Wakita[a]

Department of Virology II, National Institute of Infectious Diseases, Shinjuku-ku, Tokyo, Japan[a]; Department of Medicine and Clinical Oncology, Graduate School of Medicine, Chiba University, Chuo, Chiba, Japan[b]; Department of Virology and Liver Unit, Nagoya City University Graduate School of Medical Sciences, Kawasumi, Mizuho, Nagoya, Japan[c]; The Research Center for Hepatitis and Immunology, National Center for Global Health and Medicine, Ichikawa, Chiba, Japan[d]; and Department of Microbiology, Graduate School of Medicine, University of Tokyo, Bunkyo-ku, Tokyo, Japan[e]

To establish a cell culture system for chimeric hepatitis C virus (HCV) genotype 2b, we prepared a chimeric construct harboring the 5′ untranslated region (UTR) to the E2 region of the MA strain (genotype 2b) and the region of p7 to the 3′ UTR of the JFH-1 strain (genotype 2a). This chimeric RNA (MA/JFH-1.1) replicated and produced infectious virus in Huh7.5.1 cells. Replacement of the 5′ UTR of this chimera with that from JFH-1 (MA/JFH-1.2) enhanced virus production, but infectivity remained low. In a long-term follow-up study, we identified a cell culture-adaptive mutation in the core region (R167G) and found that it enhanced virus assembly. We previously reported that the NS3 helicase (N3H) and the region of NS5B to 3′ X (N5BX) of JFH-1 enabled replication of the J6CF strain (genotype 2a), which could not replicate in cells. To reduce JFH-1 content in MA/JFH-1.2, we produced a chimeric viral genome for MA harboring the N3H and N5BX regions of JFH-1, combined with a JFH-1 5′ UTR replacement and the R167G mutation (MA/N3H+N5BX-JFH1/R167G). This chimeric RNA replicated efficiently, but virus production was low. After the introduction of four additional cell culture-adaptive mutations, MA/N3H+N5BX-JFH1/5am produced infectious virus efficiently. Using this chimeric virus harboring minimal regions of JFH-1, we analyzed interferon sensitivity and found that this chimeric virus was more sensitive to interferon than JFH-1 and another chimeric virus containing more regions from JFH-1 (MA/JFH-1.2/R167G). In conclusion, we established an HCV genotype 2b cell culture system using a chimeric genome harboring minimal regions of JFH-1. This cell culture system may be useful for characterizing genotype 2b viruses and developing antiviral strategies.

Hepatitis C virus (HCV) is a major cause of chronic liver disease (5, 13), but the lack of a robust cell culture system to produce virus particles has hampered the progress of HCV research (2). Although the development of a subgenomic replicon system has enabled research into HCV RNA replication (15), infectious virus particle production has not been possible. Recently, an HCV cell culture system was developed using a genotype 2a strain, JFH-1, cloned from a fulminant hepatitis patient (14, 29, 32), thereby allowing investigation of the entire life cycle of this virus. However, several groups of investigators have reported genotype- and/or strain-dependent effects of some antiviral reagents (6, 17) and neutralizing antibodies (7, 25). Therefore, efficient virus production systems using various genotypes and strains are indispensable for HCV research and the development of antiviral strategies.

The JFH-1 strain is the first HCV strain that can efficiently produce HCV particles in HuH-7 cells (29). Other strains can replicate and produce infectious virus by HCV RNA transfection, but the efficiency is far lower than that of JFH-1 (24, 31). In the case of replication-incompetent strains, chimeric virus containing the JFH-1 nonstructural protein coding region is useful for analyses of viral characteristics (6, 9, 14, 23, 30, 31).

In this study, we developed a genotype 2b chimeric infectious virus production system using the MA strain (accession number AB030907) (19) harboring minimal regions of JFH-1 and cell culture-adaptive mutations that enhance infectious virus production.

MATERIALS AND METHODS

Cell culture. Huh7.5.1 cells (a kind gift from Francis V. Chisari) (32) and Huh7-25 cells (1) were cultured at 37°C in Dulbecco's modified Eagle's medium containing 10% fetal bovine serum under 5% CO_2 conditions. For follow-up study, RNA-transfected cells were passaged every 2 to 5 days depending on cell status.

Full-length genomic HCV constructs. Plasmids used in the analysis of genomic RNA replication were constructed based on pJFH1 (29) and pMA (19). For convenience, an EcoRI recognition site was introduced upstream of the T7 promoter region of pMA by PCR, and an XbaI recognition site was introduced at the end of the 3′ untranslated region (UTR). To construct MA/JFH-1, the EcoRI-BsaBI (nucleotides [nt] 1 to 2570; 5′ UTR to E2) fragment of pMA was substituted into pJFH1 (Fig. 1A). Replacement of the 5′ UTR was performed by exchanging the EcoRI-AgeI (nt 1 to 159) fragment. A point mutation in the core region (R167G) was introduced into MA chimeric constructs by PCR using the following primers: sense, 5′-TTA TGC AAC GGG GAA TTT ACC CGG TTG CTC T-3′; antisense, 5′-GGT AAA TTC CCC GTT GCA TAA TTT ATC CCG TC-3′. G167R substitution in the JFH-1 construct was performed by PCR using the following primers: sense, 5′-ATT ATG CAA CAA GGA ACC TAC CCG GTT TCC C-3′; antisense, 5′-GGT AGG TTC CTT GTT GCA TAA TTA ACC CCG TC-3′. Point mutations (L814S, R1012G, T1106A, and V1951A) were introduced into MA chimeric constructs by PCR using the following primers: L814S, 5′-GCT TAC GCC TCG GAC GCC GCT GAA CAA GGG G-3′ (sense) and 5′-AGC GGC GTC CGA GGC GTA AGC CTG CTG CGG C-3′ (antisense); R1012G, 5′-GAG GCT AGG TGG

Received 13 June 2011 Accepted 23 November 2011
Published ahead of print 7 December 2011
Address correspondence to Takaji Wakita, wakita@nih.go.jp.
* Present address: Institute of Microbial Chemistry, Shinagawa-ku, Tokyo, Japan.

doi:10.1128/JVI.05386-11

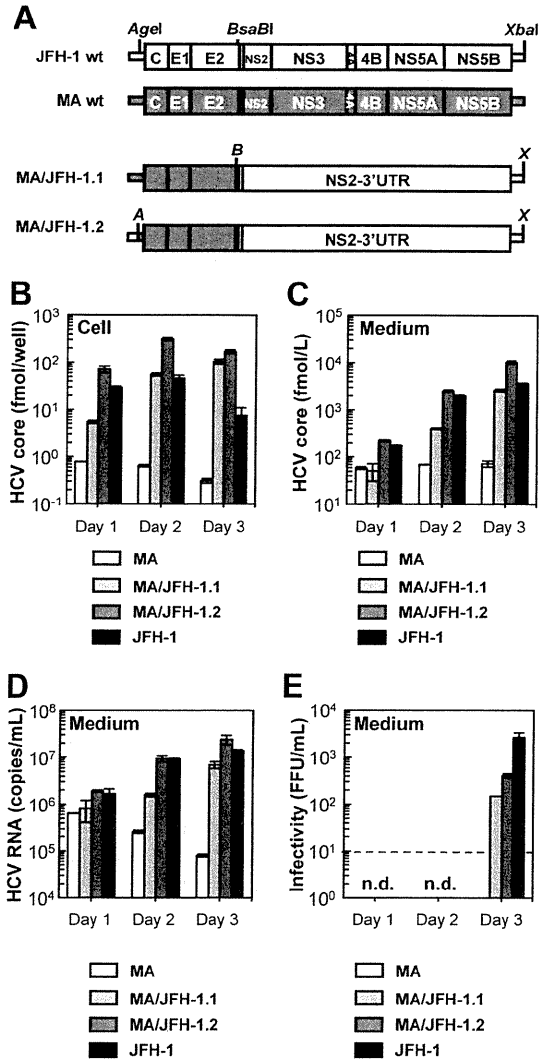

FIG 1 Replication and virus production by MA/JFH-1 chimeras in Huh7.5.1 cells. (A) Schematic structures of JFH-1, MA, and two MA/JFH-1 chimeras (MA/JFH-1.1 and MA/JFH-1.2). The junction of JFH-1 and MA in the 5′ UTR is an AgeI site, and the junction of MA and JFH-1 in the NS2 region is a BsaBI site. A, AgeI; B, BsaBI; X, XbaI. (B to E) Chimeric HCV RNA replication in Huh7.5.1 cells. HCV core protein level in cells (B) and culture medium (C) and HCV RNA levels in medium (D) and infectivity of culture medium (E) from HCV RNA-transfected Huh7.5.1 cells are shown. Ten micrograms of HCV RNA was transfected into Huh7.5.1 cells, and cells and culture medium were harvested on days 1, 2, and 3. n.d., not determined. Assays were performed three times independently, and data are presented as means ± standard deviation. Dashed line indicates detection limit. wt, wild type.

GGA AGT TCT GCT CGG CCC T-3′ (sense) and 5′-AGA ACT TCC CCA CCT AGC CTC GCG GAA ACC G-3′ (antisense); T1106A, 5′-CAG ATG TAC GCC AGC GCA GAG GGG GAC CTC-3′ (sense) and 5′-CTG CGC TGG CGT ACA TCT GGG TGA CTG GTC-3′ (antisense); and V1951A, 5′-GTG ACG CAG GCG TTA AGC TCA CTC ACA ATT ACC-3′ (sense) and 5′-TGA GCT TAA CGC CTG CGT CAC GCG CAG CGA G-3′ (antisense). To construct the MA chimeric virus harboring minimal regions of JFH-1 (MA/N3H+N5BX-JFH1), ClaI (nt 3930), EcoT22I (nt 5294), and BsrGI (nt 7782) recognition sites were introduced into pMA by site-directed mutagenesis. The 5′ UTR (EcoRI-AgeI), the region of the NS3 helicase (N3H; ClaI-EcoT22I), and the region of NS5B to 3′ X (N5BX; BsrGI-XbaI) were then replaced with the corresponding regions from JFH-1.

RNA synthesis, transfection, and determination of infectivity. RNA synthesis and transfection were performed as described previously (12, 22). Determination of infectivity was also performed as described previously, with infectivity expressed as the number of focus-forming units per milliliter (FFU/ml) (12, 22). When necessary, culture medium was concentrated 20-fold in Amicon Ultra-15 spin columns (100-kDa molecular-weight-cutoff; Millipore, Bedford, MA) in order to determine infectivity.

Quantification of HCV core protein and HCV RNA. In order to estimate the concentration of HCV core protein in culture medium, we performed a chemiluminescence enzyme immunoassay (Lumipulse II HCV core assay; Fujirebio, Tokyo, Japan) in accordance with the manufacturer's instructions. HCV RNA from harvested cells or culture medium was isolated using an RNeasy Mini RNA kit (Qiagen, Tokyo, Japan) or QiaAmp Viral RNA Minikit (Qiagen), respectively. Copy number of HCV RNA was determined by real-time quantitative reverse transcription-PCR (qRT-PCR), as described previously (28).

HCV sequencing. Total RNA in culture supernatant was extracted with Isogen-LS (Nippon Gene Co., Ltd., Tokyo, Japan). cDNA was synthesized using Superscript III Reverse Transcriptase (Invitrogen, Carlsbad, CA). cDNA was subsequently amplified with LA *Taq* DNA polymerase (TaKaRa, Shiga, Japan). Four separate PCR primer sets were used to amplify the fragments of nt 130 to 2909, 2558 to 5142, 4784 to 7279, and 7081 to 9634 covering the entire open reading frame and part of the 5′ UTR and 3′ UTR of the MA strain. Sequences of amplified fragments were determined directly.

Immunostaining. Infected cells were cultured on Multitest Slides (MP Biomedicals, Aurora, OH) and were fixed in acetone-methanol (1:1, vol/vol) for 15 min at −20°C. After a blocking step, infected cells were visualized with anti-core protein antibody (clone 2H9) (29) and Alexa Fluor 488 goat anti-mouse IgG (Invitrogen), and nuclei were visualized with 4′,6′-diamidino-2-phenylindole (DAPI).

Assessment of interferon sensitivity. Two micrograms of *in vitro* transcribed RNA was transfected into 3×10^6 Huh7.5.1 cells. Four hours after transfection, cells were placed in fresh medium or medium containing 0.1, 1, 10, 100, and 1,000 IU/ml of interferon α-2b (Intron A; Schering-Plough Corporation, Osaka, Japan). Culture medium was then harvested on day 3, and HCV core levels in the cells and in the medium were measured.

Statistical analysis. Significant differences were evaluated by Student's *t* test. A *P* value of <0.05 was considered significant.

RESULTS

Transient replication and production of 2b/2a chimeric virus. We first tested whether the MA strain (genotype 2b) (19) was able to replicate and produce infectious virus in cultured cells. When the *in vitro* transcribed RNA of MA was transfected into Huh7.5.1 cells, a highly HCV-permissive cell line, replication and virus production were not observed (Fig. 1A to C). We then tested whether 2b/2a chimeric RNA harboring the structural region (5′ UTR to E2) of the MA strain and the nonstructural region (p7 to 3′ UTR) of JFH-1 (Fig. 1A, MA/JFH-1.1) was able to replicate in the cells. After MA/JFH-1.1 RNA transfection, time-dependent accumulation of core protein in the cells (Fig. 1B) and culture medium (Fig. 1C) was observed, indicating that MA/JFH-1.1 RNA was able to replicate in the cells autonomously. HCV RNA levels in the medium were determined by qRT-PCR, and time-dependent increases in HCV RNA level were also observed (Fig. 1D). Infectious virus production was observed on day 3, but infectivity was 17.6-fold lower than that of JFH-1 (Fig. 1E).

In order to improve the level of infectious virus production, we tested another chimeric construct, MA/JFH-1.2, which contained an additional MA-to-JFH-1 replacement of the 5′ UTR (Fig. 1A),

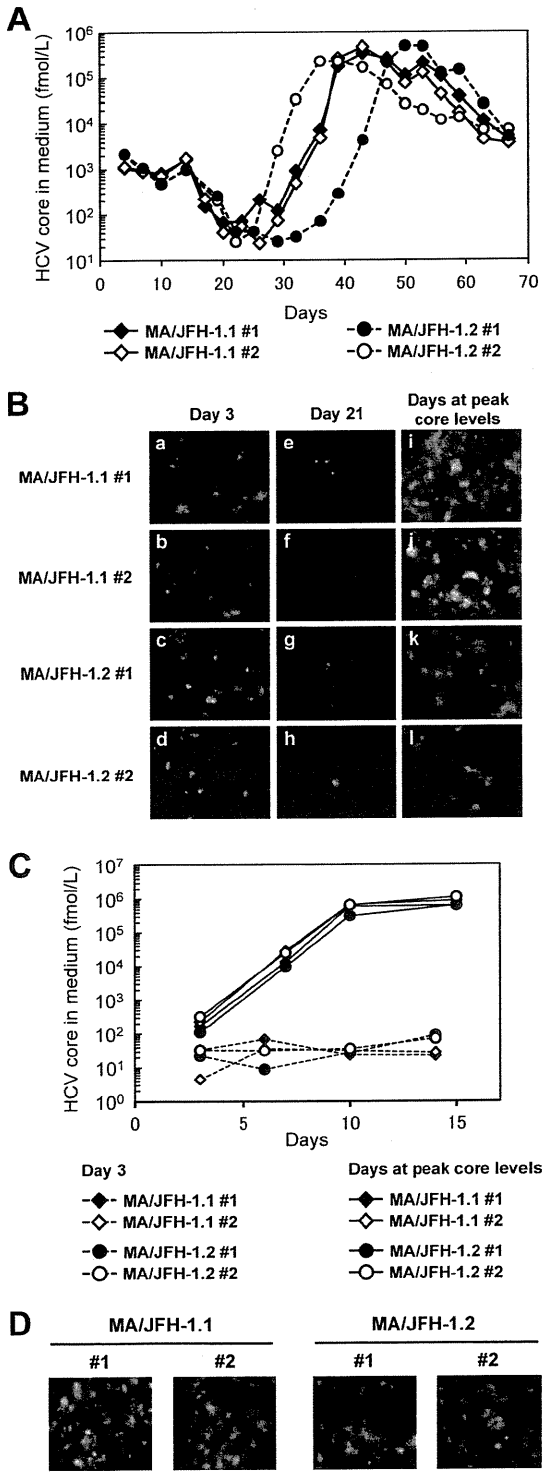

FIG 2 Long-term culture of MA/JFH-1.1 and MA/JFH-1.2 RNA-transfected cells. Ten micrograms of HCV RNA was transfected into Huh7.5.1 cells, and cells were passaged every 2 to 5 days, depending on cell status. Culture medium was collected after every passage, and HCV core protein levels were measured. Transfection was performed twice for each chimeric RNA (1 and 2 for each construct). (A) HCV core protein levels in culture medium from MA/JFH-1.1 and MA/JFH-1.2 RNA-transfected cells. (B) Immunostained cells at 3 days after transfection (a to d), at 21 days after transfection (e to h), and at the time of peak core levels (days 42 to 49). Infected cells were visualized with anti-core protein antibody (green), and nuclei were visualized with DAPI (blue). (C) Infection of naïve cells by culture medium at an MOI of 0.001. (D) Immunostained cells at 15 days after infection with medium at peak core protein levels (Fig. 2A) at an MOI of 0.001. Infected cells were visualized with anti-core antibody (green), and nuclei were visualized with DAPI (blue).

TABLE 1 HCV core protein levels and infectivity in culture medium immediately after RNA transfection (day 3) and after long-term culture (days 35 to 49)

Sample period and virus	Sample no.	Day no.[a]	HCV core (fmol/liter)	Infectivity (FFU/ml)
After transfection				
MA/JFH-1.1	1	3	1.06×10^3	5.00×10^1
	2	3	1.14×10^3	5.70×10^1
MA/JFH-1.2	1	3	2.14×10^3	7.30×10^1
	2	3	2.15×10^3	9.30×10^1
After long-term culture				
MA/JFH-1.1	1	42	3.38×10^5	1.62×10^5
	2	42	4.70×10^5	3.23×10^5
MA/JFH-1.2	1	35	2.27×10^5	1.61×10^5
	2	49	4.93×10^5	3.27×10^5

[a] For the long-term culture, the days are those of peak core protein levels.

as a 5′ UTR replacement from J6CF (genotype 2a) to JFH-1 enhanced virus production of chimeric J6CF virus harboring the region of NS2 to 3′ X of JFH-1 (J6/JFH-1) (A. Murayama et al., unpublished data). The core protein accumulation levels with MA/JFH-1.2 RNA-transfected cells were higher than those with MA/JFH-1.1 ($P < 0.05$) (Fig. 1B). Similarly, core protein and HCV RNA levels in the medium of MA/JFH-1.2 RNA-transfected cells were higher than those of MA/JFH-1.1 ($P < 0.05$) (Fig. 1C and D). Infectivity on day 3 was also higher than with MA/JFH-1.1 ($P < 0.05$) (Fig. 1E), indicating that the 5′ UTR of JFH-1 enhanced virus production. However, infectivity of medium from MA/JFH-1.2 RNA-transfected cells on day 3 remained 6.4-fold lower than that of JFH-1 although HCV RNA levels in the medium were similar to those of JFH-1 (Fig. 1D and E).

These results indicate that 2b/2a chimeric RNA is able to replicate autonomously in Huh7.5.1 cells and produce infectious virus although infectivity remains lower than that of JFH-1.

Assembly-enhancing mutation in core region introduced during long-term culture. Because MA/JFH-1.1 and MA/JFH-1.2 replicated efficiently but produced small amounts of infectious virus, we performed long-term culture of these RNA-transfected cells in order to examine whether these chimeric RNAs would continue replicating and producing infectious virus over the long term. We prepared two RNA-transfected cell lines for each construct (MA/JFH-1.1 and MA/JFH-1.2) as both of these replicated and produced infectious virus at different levels.

Immediately after transfection, core protein levels and infectivity in culture medium were low (1.06×10^3 to 2.15×10^3 fmol/liter and 5.00×10^1 to 9.30×10^1 FFU/ml, respectively) (Fig. 2A and Table 1) although a considerable number of core protein-positive cells were observed by immunostaining (Fig. 2B, frames a to d). Subsequently, core protein levels in the culture medium decreased gradually (Fig. 2A), and core protein-positive cells were rare (Fig. 2B, frames e to h). However, at 30 to 40 days

after transfection, core protein levels in the supernatants of all chimeric RNA-transfected cells increased and reached 2.27×10^5 to 4.93×10^5 fmol/liter (Fig. 2A and Table 1). Infectivity in the culture medium also increased (1.61×10^5 to 3.27×10^5 FFU/ml) (Table 1), and at this point, most of the cells were core protein positive (Fig. 2B, frame i to l).

As the infectivity of culture supernatant of MA/JFH-1 RNA-transfected cells appeared to increase after long-term culture, we compared viral spread by infection with these supernatants on day 3 (immediately after transfection) and for each peak in core protein levels (after long-term culture). When naïve Huh7.5.1 cells were infected with supernatant on days corresponding to a peak in core protein levels at a multiplicity of infection (MOI) of 0.001, core protein levels in the medium increased rapidly and reached 0.64×10^6 to 1.13×10^6 fmol/liter by day 15 after infection (Fig. 2C). Immunostained images showed that most cells were HCV core protein positive on day 15 (Fig. 2D). When naïve Huh7.5.1 cells were infected with supernatant from day 3 at an MOI of 0.001, core protein levels in the medium did not increase under these conditions (Fig. 2C). These results indicate that both MA/JFH-1 chimeric viruses (MA/JFH-1.1 and MA/JFH-1.2) acquired the ability to spread rapidly after long-term culture.

As the characteristics of the MA/JFH-1 virus changed in long-term culture, we analyzed the possible mutations in the viral genome from the supernatant at each peak in core protein levels (Table 1, days at peak core levels). Nine- to 12-nucleotide mutations were found in the viral genome from each supernatant, and the detected mutations were distributed along the entire genome. Among these mutations, a common nonsynonymous mutation was found in the core region (Arg to Gly at amino acid [aa]167, R167G).

In order to test the effects of R167G on virus production, an R167G substitution was introduced into MA/JFH-1.2 as MA/JFH-1.2 replicated and produced infectious virus more efficiently than MA/JFH-1.1. HCV core protein levels in cells and medium of MA/JFH-1.2 with R167G (MA/JFH-1.2/R167G) were higher than with MA/JFH-1.2 ($P < 0.05$) (Fig. 3A and B). HCV RNA levels in the medium of MA/JFH-1.2/R167G RNA-transfected cells were also higher than with MA/JFH-1.2 ($P < 0.05$) (Fig. 3C). Infectious virus production was also increased by the R167G mutation ($P < 0.05$) (Fig. 3D) and was 8.7-fold higher than that of JFH-1 RNA-transfected cells on day 3 ($P < 0.05$) (Fig. 3D).

We then tested whether R167G was responsible for the rapid spread observed in culture supernatant after long-term culture by monitoring virus spread after infection of naïve Huh7.5.1 with culture medium taken 3 days after RNA transfection of MA/JFH-1.2 and MA/JFH-1.2/R167G at an MOI of 0.005. Core protein levels in medium from MA/JFH-1.2/R167G-infected cells increased with the same kinetics as levels of JFH-1 (Fig. 3E), and the population of core protein-positive cells was almost the same as with JFH-1-infected cells (Fig. 3F), indicating that MA/JFH-1.2/R167G virus spread as rapidly as JFH-1 virus. In contrast, we observed no infectious foci in the MA/JFH-1.2 virus-inoculated cells (Fig. 3F). These data suggest that the R167G mutation in the core region was a cell culture-adaptive mutation and that it enhanced infectious MA/JFH-1.2 virus production.

In order to determine whether R167G enhances RNA replication or other steps in the viral life cycle, we performed a single-cycle virus production assay (11) using Huh7-25 cells, a Huh-7-derived cell line lacking CD81 expression on the cell surface (1).

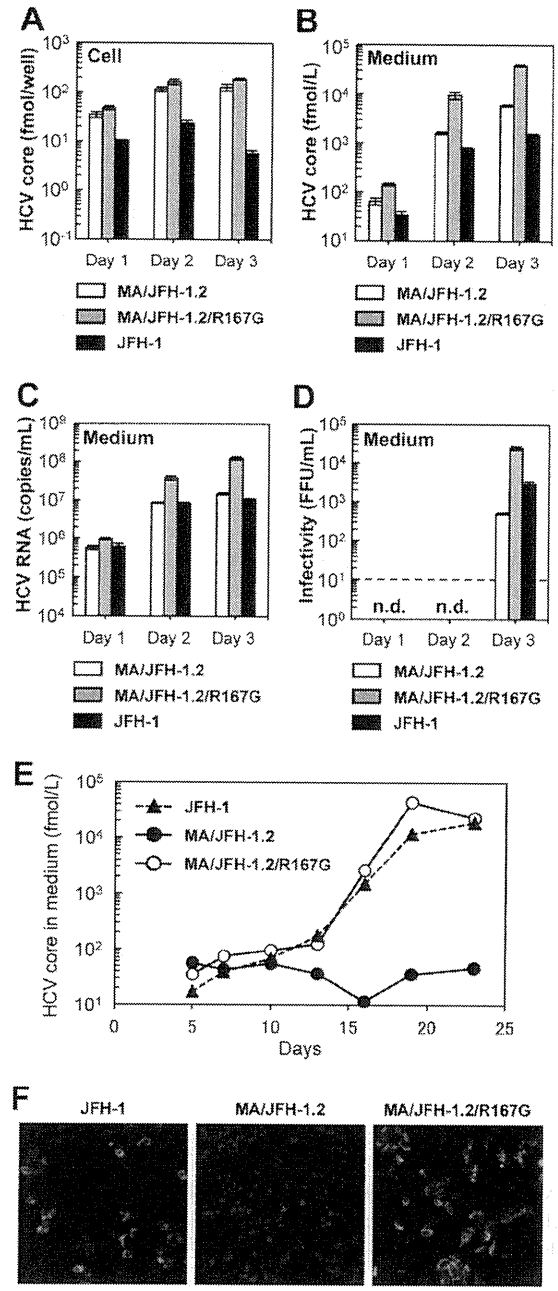

FIG 3 Effects of R167G on replication and virus production of MA/JFH-1.2 in Huh7.5.1 cells. Ten micrograms of HCV RNA was transfected into Huh7.5.1 cells, and cells and medium were harvested on days 1, 2, and 3. HCV core protein levels in the cells (A) and culture medium (B) and HCV RNA levels in the medium (C) and the infectivity of culture medium (D) from HCV RNA-transfected Huh7.5.1 cells are shown. n.d., not determined. Dashed line indicates the detection limit. Assays were performed three times independently, and data are presented as means ± standard deviation. (E) HCV core protein levels in culture medium from cells infected with medium at 3 days posttransfection at an MOI of 0.005. (F) Immunostained cells at 19 days postinfection. Infected cells were visualized with anti-core antibody (green), and nuclei were visualized with DAPI (blue).

This cell line can support replication and infectious virus production upon transfection of HCV genomic RNA but cannot be reinfected by progeny virus, thereby allowing observation of a single cycle of infectious virus production without the confounding ef-

fects of reinfection. R167G did not affect HCV core protein levels in the chimeric RNA-transfected Huh7-25 cells (Fig. 4A), demonstrating that R167G did not enhance RNA replication. Nevertheless, R167G increased HCV core protein levels in the medium ($P < 0.05$ on days 2 and 3) and infectivity (Fig. 4B and C). These results suggest that R167G did not affect RNA replication but affected other steps such as virus assembly and/or virus secretion.

Virus particle assembly efficiency was then assessed by determining intracellular-specific infectivity from infectivity and RNA titer in the cells, as reported previously (11). As shown in Fig. 4G, R167G enhanced intracellular-specific infectivity of MA/JFH-1.2 virus 10.2-fold. Virus secretion efficiency was also calculated from the amount of intracellular and extracellular infectious virus, but R167G had no effect (Fig. 4G).

To confirm the effects of Arg167 in other HCV strains, we tested its effects on JFH-1. As aa 167 of JFH-1 is Gly, we replaced it with Arg (G167R). HCV core protein levels in the cells were not affected by G167R (Fig. 4D), and no effects on RNA replication were confirmed. HCV core protein levels in the medium and infectivity decreased after G167R mutation (Fig. 4E and F). As the G167R mutation decreased intracellular infectious virus production of JFH-1 to undetectable levels, we were unable to determine the intracellular-specific infectivity and virus secretion efficiency of JFH-1 G167R (Fig. 4G). These results indicate that Gly is favored over Arg at core position 167 for infectious virus assembly in multiple HCV strains.

MA harboring the R167G mutation, 5′ UTR, and N3H (NS3 helicase) and N5BX (NS5B to 3′ X) regions of JFH-1 replicated and produced infectious chimeric virus. In order to establish a genotype 2b cell culture system with the MA strain with minimal regions of JFH-1, we attempted to reduce JFH-1 content in MA/JFH-1.2. We previously reported that replacement of the N3H and N5BX regions of JFH-1 allowed efficient replication of the J6CF strain, which normally cannot replicate in cells (21). Thus, we tested whether the N3H and N5BX regions of JFH-1 could also support MA RNA replication.

We prepared two chimeric MA constructs harboring the 5′ UTR and N3H and N5BX regions of JFH-1, MA/N3H+N5BX-JFH1 (Fig. 5A) and MA/N3H+N5BX-JFH1/R167G. After *in vitro* transcribed RNA was transfected into Huh7.5.1 cells, intracellular core protein levels of MA/N3H+N5BX-JFH1 and MA/N3H+N5BX-JFH1/R167G RNA-transfected cells increased in a time-dependent manner and reached almost the same levels as with MA/JFH-1.2 RNA-transfected cells on day 5 (Fig. 5B). Extracellular core protein and HCV RNA levels of MA/N3H+N5BX-JFH1 and MA/N3H+N5BX-JFH1/R167G RNA-transfected cells also increased in a time-dependent manner (Fig. 5C and D). However, they were more than 10 times lower than with MA/JFH-1.2 RNA-transfected cells although intracellular core levels were comparable on day 5 (Fig. 5B to D).

We then tested whether the medium from MA/N3H+N5BX-JFH1 and MA/N3H+N5BX-JFH1/R167G RNA-transfected cells was infectious. Infectivity of the medium from MA/N3H+N5BX-JFH1 RNA-transfected cells was below the detection limit, and that of MA/N3H+N5BX-JFH1/R167G RNA-transfected cells on day 5 was very low ($3.3 \times 10^1 \pm 2.1 \times 10^1$ FFU/ml) (Fig. 5E). To confirm infectivity, the culture media were concentrated, and their infectivity was determined. Infected foci were observed after infection with concentrated medium in MA/N3H+N5BX-JFH1/R167G RNA-transfected cells (Fig. 5F), and infectivity was found

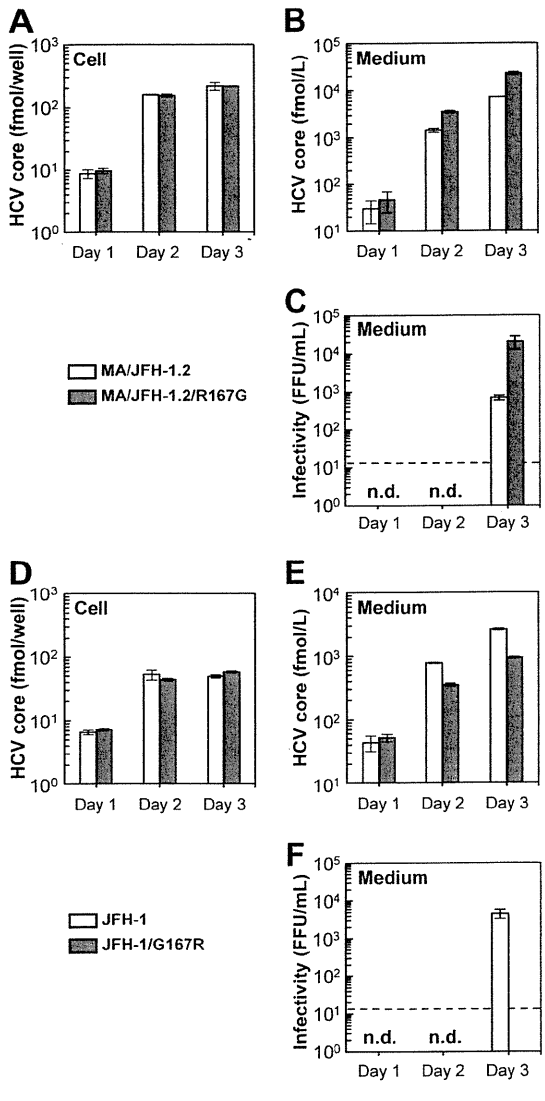

G

Construct	Intracellular Specific Infectivity (FFU/ x10⁶ HCV RNA copies)	Infectious Virus Secretion (Extra/Intra)
MA/JFH-1.2	1.68 ± 0.404	20.2 ± 4.26
MA/JFH-1.2/R167G	17.1 ± 4.38	14.1 ± 1.65
JFH-1	1.78 ± 0.364	63.3 ± 6.44
JFH-1/G167R	NA	NA

FIG 4 Effects of R167G on replication and virus production of MA/JFH-1.2 and JFH-1 in Huh7-25 cells. Ten micrograms of HCV RNA was transfected into Huh7-25 cells, and cells and medium were harvested on days 1, 2, and 3. HCV core protein levels in cells (A and D) and in medium (B and E) were measured, and infectivity of medium (C and F) was determined. n.d., not determined. Dashed line indicates the detection limit. (G) Intracellular specific infectivity and virus secretion efficiency of chimeric HCV RNA-transfected cells. Intracellular and extracellular infectivity of day 3 samples was determined, and specific infectivity and virus secretion rate were calculated. Assays were performed three times independently, and data are presented as means ± standard deviation. NA, not available.

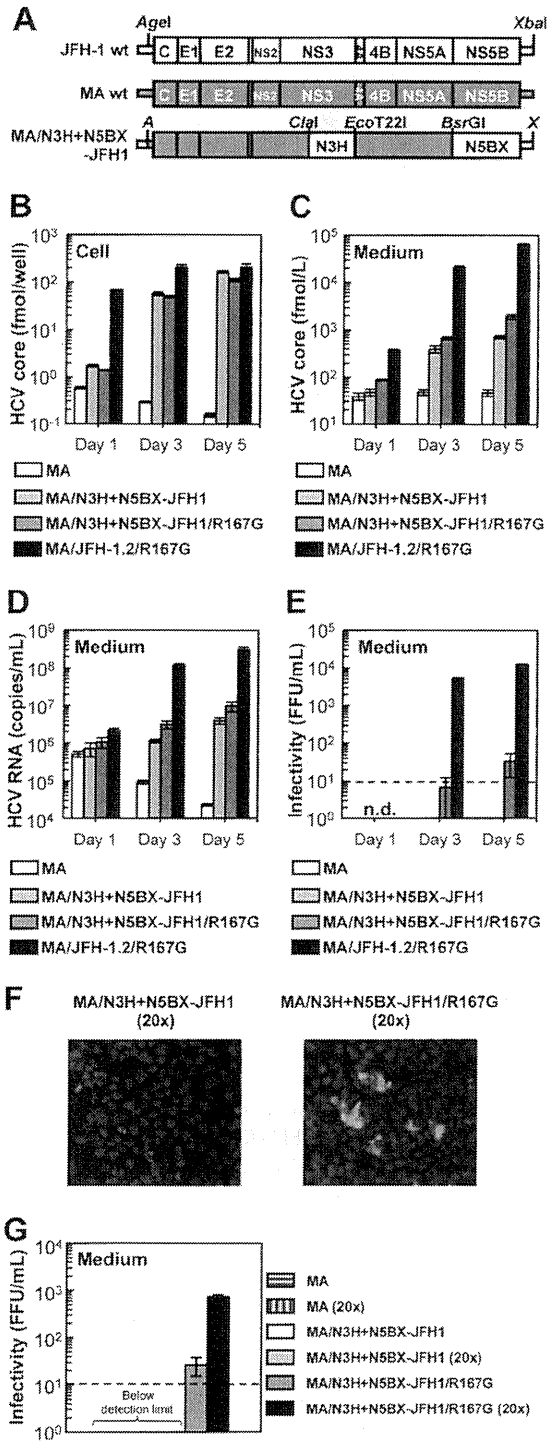

FIG 5 Replication and virus production of MA/N3H+N5BX-JFH1/R167G in Huh7.5.1 cells. (A) Schematic structures of JFH-1, MA, and MA/N3H+N5BX-JFH1. The junction of JFH-1 and MA in the 5′ UTR is an AgeI site; the junctions of MA and JFH-1 in the NS3 regions are ClaI and EcoT22I sites, and the junction in the NS5B region is a BsrGI site. A, AgeI; X, XbaI. (B to G) Chimeric HCV RNA replication in Huh7.5.1 cells. Ten micrograms of HCV RNA was transfected into Huh7.5.1 cells, and cells and medium were harvested on days 1, 3, and 5. HCV core protein levels in cells (B) and in medium (C) and HCV RNA levels in medium (D) were measured, and infectivity of medium (E) was determined. Assays were performed three times independently, and data are presented as means ± standard deviation. n.d., not determined. Dashed line indicates the detection limit. (F) Immunostained cells. Huh7.5.1 cells were infected with concentrated medium from RNA-transfected cells on day 5. Infected cells were visualized with anti-core antibody (green), and nuclei were visualized with DAPI (blue). (G) Infectivity of concentrated culture medium from HCV RNA-transfected cells. Culture medium was concentrated by 20 times. Infectivities of original and concentrated culture media were determined. Dashed line indicates detection thelimit.

to be $7.27 \times 10^2 \pm 7.57 \times 10^1$ FFU/ml (Fig. 5G). No infected foci were observed after infection of MA/N3H+N5BX-JFH1 RNA-transfected cells, even when medium was concentrated (Fig. 5F), although intracellular and extracellular core protein levels were comparable to those with MA/N3H+N5BX-JFH1/R167G RNA-transfected cells (Fig. 5B and C). These results indicate that replacement of the 5′ UTR and N3H and N5BX regions in JFH-1 were necessary to rescue autonomous replication in the replication-incompetent MA strain and for secretion of infectious chimeric virus. However, the secretion and infection efficiencies of the virus were low.

Cell culture-adaptive mutations enhanced infectious virus production of MA/N3H+N5BX-JFH1/R167G. Because MA/N3H+N5BX-JFH1/R167G replicated efficiently but produced very small amounts of infectious virus, we performed a long-term culture of the RNA-transfected cells in order to induce cell culture-adaptive mutations that could enhance infectious virus production. We prepared RNA-transfected cells using two constructs, MA/N3H+N5BX-JFH1 and MA/N3H+N5BX-JFH1/R167G; both of these replicated efficiently, and MA/N3H+N5BX-JFH1/R167G produced infectious virus at low levels while MA/N3H+N5BX-JFH1 did not. Immediately after transfection, the HCV core protein levels in the medium of each RNA-transfected cell culture peaked at 3.0×10^3 fmol/liter and declined thereafter. However, the core protein level in the medium with MA/N3H+N5BX-JFH1/R167G RNA-transfected cells continued to increase and reached a peak of 2.7×10^5 fmol/liter 54 days after transfection, at which point most cells were core protein positive (Fig. 6B). The core protein level in the medium with MA/N3H+N5BX-JFH1 RNA-transfected cells did not increase and core-positive cells were scarce on day 54 (Fig. 6B). We analyzed the viral genome in the culture supernatants from day 54 for possible mutations and identified four nonsynonymous mutations in the MA/N3H+N5BX-JFH1/R167G genome: L814S (NS2), R1012G, (NS2), T1106A (NS3), and V1951A (NS4B). In order to test whether these amino acid substitutions enhance infectious virus production, L814S, R1012G, T1106A, and V1951A were introduced into MA/N3H+N5BX-JFH1/R167G, and the product was designated MA/N3H+N5BX-JFH1/5am (where am indicates adaptive mutation). On day 1, although HCV core protein levels in the MA/N3H+N5BX-JFH1/5am RNA-transfected cells were higher than those of MA/N3H+N5BX-JFH1/R167G RNA-transfected cells, they were still lower than those of MA/JFH-1.2/R167G RNA-transfected cells; however, on days 3 and 5, they reached a level comparable to that of MA/JFH-1.2/R167G RNA-transfected cells (Fig. 6C). HCV core protein and HCV RNA levels in the medium of MA/N3H+N5BX-JFH1/5am RNA-transfected cells were higher than those of MA/JFH-1.2/R167G RNA-transfected cells ($P < 0.05$, Fig. 6D and 6E, respectively). MA/N3H+N5BX-JFH1/5am, containing the four additional adaptive mutations, produced infectious virus at the same level as MA/JFH-1.2/R167G on day 5 (Fig. 6F). These results indicate that the

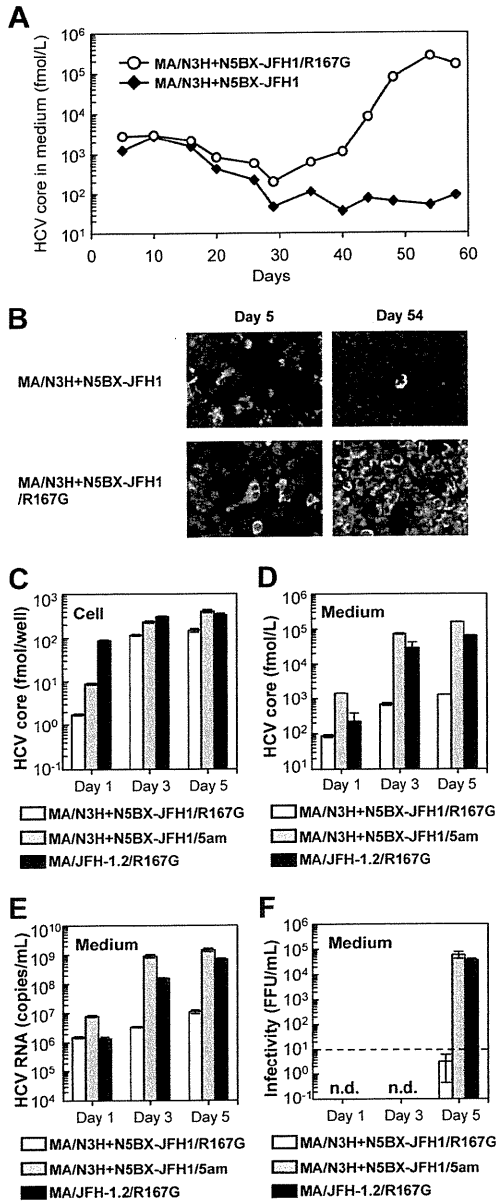

FIG 6 Cell culture-adaptive mutations enhanced infectious virus production of MA/N3H+N5BX-JFH1/R167G. (A) Long-term culture of MA/N3H+N5BX-JFH1 and MA/N3H+N5BX-JFH1/R167G RNA-transfected cells. Ten micrograms of HCV RNA was transfected into Huh7.5.1 cells, and cells were passaged every 2 to 5 days, depending on cell status. Culture medium was collected after every passage, and HCV core protein levels were measured. HCV core protein levels in culture medium from MA/N3H+N5BX-JFH1 and MA/N3H+N5BX-JFH1/R167G RNA-transfected cells are presented. (B) Immunostained cells on days 5 and 54 after transfection. Infected cells were visualized with anti-core antibody (green), and nuclei were visualized with DAPI (blue). (C to F) Effect of four additional cell culture-adaptive mutations on virus production. Ten micrograms of HCV RNA was transfected into Huh7.5.1 cells, and cells and medium were harvested on days 1, 3, and 5. HCV core levels in cells (C) and in medium (D) and HCV RNA levels in medium (E) were measured, and infectivity of medium (F) was determined. Assays were performed three times independently, and data are presented as means ± standard deviation. n.d., not determined. Dashed line indicates the detection limit.

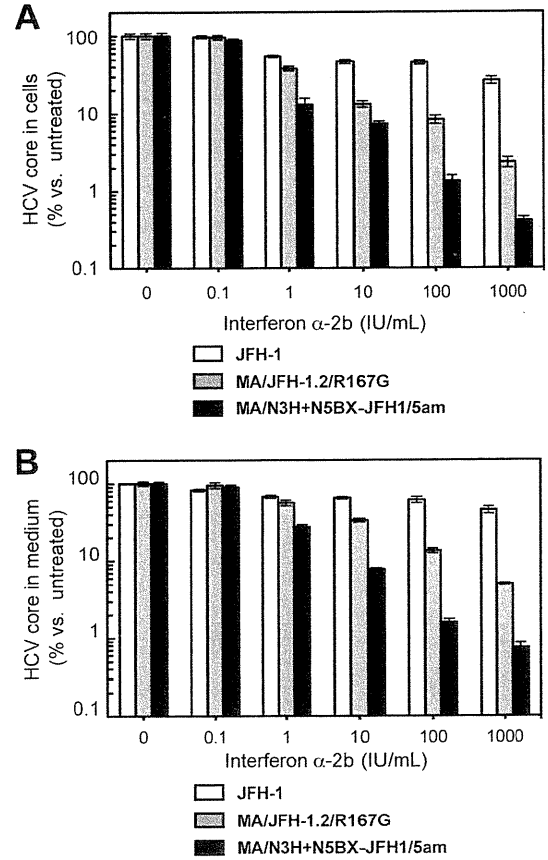

FIG 7 Comparisons of interferon sensitivity between JFH-1, MA/JFH-1.2/R167G and MA/N3H+N5BX-JFH1/5am. Two micrograms of HCV RNA was transfected into Huh7.5.1 cells, and interferon was added at the indicated concentrations at 4 h after transfection. HCV core protein levels in cells (A) and in medium (B) on day 3 were measured, and data are expressed as percent versus untreated cells (0 IU/ml). Assays were performed three times independently, and data are presented as means ± standard deviation.

four additional adaptive mutations enhance infectious virus production and that MA/N3H+N5BX-JFH1/5am RNA-transfected cells replicate and produce infectious virus as efficiently as MA/JFH-1.2/R167G RNA-transfected cells.

Comparison of interferon sensitivity between JFH-1, MA/JFH-1.2/R167G, and MA/N3H+N5BX-JFH1/R167G. Using the newly established genotype 2b infectious chimeric virus, we compared interferon sensitivity between the JFH-1, MA/JFH-1.2/R167G, and MA/N3H+N5BX-JFH1/5am viruses. JFH-1 or MA chimeric viral RNA-transfected Huh7.5.1 cells were treated with 0.1, 1, 10, 100, or 1,000 IU/ml interferon α-2b, and HCV core protein levels in the cells and in culture media were compared. Interferon decreased HCV core protein levels in the JFH-1 RNA-transfected cells and in the medium in a dose-dependent manner, and production was inhibited to 26.8% ± 3.0% and 45.6% ± 4.7%, respectively, of control levels (Fig. 7A and B, respectively). In contrast, HCV core protein levels in cells and medium of MA/JFH-1.2/R167G and MA/N3H+N5BX-JFH1/5am RNA-transfected cells decreased more pronouncedly in a dose-dependent manner (Fig. 7A and B, respectively). HCV core protein levels in cells and medium from MA/N3H+N5BX-JFH1/5am RNA-transfected cells were lower than those from MA/JFH-1.2/

R167G RNA-transfected cells (Fig. 7A and B, respectively) ($P < 0.05$ at 1, 10, 100, and 1,000 IU/ml), indicating that the MA/N3H+N5BX-JFH1/5am virus was more sensitive to interferon than the MA/JFH1.2/R167G virus, which contained more regions from JFH-1.

DISCUSSION

In this study, we developed a novel infectious HCV production system using a genotype 2b chimeric virus. To improve infectious virus production, we introduced two modifications into the chimeric genome.

First, we replaced the 5′ UTR from MA with that of JFH-1. Similarly to J6/JFH-1, replacement of the 5′ UTR increased core protein accumulation in both the cells and medium when these RNAs were transfected into Huh7.5.1 cells (Fig. 1). The same trend was observed when these RNAs were transfected into Huh7-25 cells (data not shown), indicating that the 5′ UTR of JFH-1 enhanced RNA replication. There are two genetic variations in J6CF and seven in MA in the region we replaced (nt 1 to 154 for J6CF and nt 1 to 155 for MA), and some of these mutations may affect RNA replication by changing the RNA secondary structure, RNA-RNA interactions, or binding of host or viral proteins.

Second, we introduced a cell culture-adaptive mutation (R167G) in the core region. This mutation was induced by long-term culture of MA/JFH-1 RNA-transfected cells (Fig. 2). MA/JFH-1 chimeric RNA (MA/JFH-1.1 and MA/JFH-1.2) replicated when synthesized RNA was transfected into the cells. However, infectious virus production was low, and virus infection did not spread over the short term. In early stages of long-term culture, the number of core protein-positive cells gradually decreased, and core protein-positive cells were scarcely detectable. Subsequently, the population of core protein-positive cells increased, reaching almost 100%. At this time point, we identified a common mutation in the core region (R167G) of the viral genome as a cell culture-adaptive mutation and found that it enhanced infectious virus production (Fig. 3). Several nonsynonymous mutations other than R167G were identified in the viral genome from each supernatant, and these mutations may enhance infectious virus production. However, there was a discrepancy between RNA levels and the infectivity of the culture media of MA/JFH-1.2 and MA/JFH-1.2/R167G RNA-transfected cells (Fig. 3C and D). The MA/JFH-1.2/R167G mutant had a 2-log increase in viral infectivity compared to that of MA/JFH-1.2 but only a 1-log increase in secreted RNA. The replication efficiency of MA/JFH-1.2 RNA-transfected cells was comparable to that of MA/JFH-1.2/R167G RNA-transfected cells, but the efficiency of infectious virus assembly within the cells was low, indicating that mainly noninfectious virus may be produced.

Infection of MA/JFH-1.2/R167G virus spreads rapidly, similarly to that of the JFH-1 virus, when it is inoculated into naïve Huh7.5.1 cells. On a single-cycle virus production assay, we found that the R167G mutation did not affect RNA replication or virus secretion but enhanced infectious virus assembly within the cells (Fig. 4). Efficient infectious virus assembly within the cells was mainly responsible for the rapid spread and high virus production of MA/JFH-1.2/R167G.

The amino acid at 167 (aa 167) is located in domain 2 of the core region, which is important for localization of the core protein (3, 8). Lipid droplet localization of the core protein and/or NS5A is important for infectious virus production (4, 18, 26). The interaction between the core protein and NS5A is also important for infectious virus production (16). Thus, aa 167 affects infectious virus production possibly by altering subcellular localization of the core protein or interaction between the core protein and NS5A. We examined the amino acid sequence of the core protein in 2,078 strains in the Hepatitis Virus Database (http://s2as02.genes.nig.ac.jp/) and found that aa 167 is Gly in all other strains. These data strongly suggest that Gly at aa 167 is important for the HCV life cycle. As the MA strain was cloned from the serum of a patient with chronic hepatitis C, the low virus production by this Gly at aa 167 may be important for persistent infection.

We then attempted to reduce the contents of JFH-1 from MA/JFH-1.2/R167G. We previously reported that the N3H and N5BX regions of JFH-1 were sufficient for replication of the J6CF strain (21). We also reported that this effect was observed only in genotype 2a strains (J6CF, JCH-1, and JCH-4). In this study, we tested whether the N3H and N5BX regions of JFH-1 could also support replication of a genotype 2b strain, MA. We constructed an MA chimeric virus harboring the N3H and N5BX regions of JFH-1 and combined this with the 5′ UTR of JFH-1 and the R167G mutation (MA/N3H+N5BX-JFH1/R167G). This chimeric RNA was able to replicate in the cells and produce infectious chimeric virus in culture medium although infectious virus production levels were low (Fig. 5).

We showed in this paper that the N3H and N5BX regions of JFH-1 were able to support RNA replication by both genotype 2a clones and genotype 2b clones, but the nucleotide sequence similarity between JFH-1 and MA was lower than that between JFH-1 and J6CF (77% versus 89%, respectively). Compared to MA/JFH-1.2/R167G, MA/N3H+N5BX-JFH1/R167G RNA showed the same levels of RNA replication and low levels of infectious virus production. To clarify whether there were any differences in the characteristics of the secreted virus, we performed density gradient ultracentrifugation with the MA/JFH-1.2/R167G and MA/N3H+N5BX-JFH1/R167G viruses. The distributions of the HCV core protein and infectivity showed similar profiles (data not shown).

The differences between MA/JFH-1.2/R167G and MA/N3H+N5BX-JFH1/R167G are the NS2, NS3 protease domain (N3P), and NS4A to NS5A regions. Nucleotide variation(s) other than aa 167 in these regions of the MA strain may be associated with reduced virus assembly. We identified four additional cell culture-adaptive mutations, L814S (NS2), R1012G (NS2), T1106A (NS3), and V1951A (NS4B), which resulted from long-term culture of MA/N3H+N5BX-JFH1/R167G RNA-transfected cells. Consequently, cells transfected with MA/N3H+N5BX-JFH1/5am constructed by insertion of these four adaptive mutations into MA/N3H+N5BX-JFH1/R167G replicated and produced infectious virus as efficiently as MA/JFH-1.2/R167G RNA-transfected cells (Fig. 6).

This system is able to contribute to studies into the development of antiviral strategies. It has been reported that HCV genotype 2a was more sensitive to interferon therapy than HCV genotype 2b in a clinical study (20). To assess the interferon resistance of genotype 2b, a cell culture system with multiple genotype 2b strains is necessary. The previously reported replicable genotype 2b chimeric virus harbored only structural

regions of 2b strains (6, 27). The 2b/JFH-1 chimeric virus containing the region of the core protein to NS2 from the J8 strain (genotype 2b) and the region of NS3 to 3′ X of JFH-1 was able to replicate and showed that there were no differences in interferon sensitivity among the JFH-1 chimeric viruses of other genotypes (6, 27). Another 2b/JFH-1 chimeric virus containing the regions of the core protein to NS2 (nt 342 to 2867) of a genotype 2b strain and of NS2 to 3′ UTR (nt 2868) of JFH-1 has been reported (6, 27). The authors reported that their 2b/JFH-1 chimeric virus was more sensitive to interferon than JFH-1 (6, 27). We developed the genotype 2b HCV cell culture system with another HCV genotype 2b strain (MA). We identified a virus assembly-enhancing mutation in the core region, the minimal JFH-1 regions necessary for replication, and four additional adaptive mutations that enhance infectious virus production and demonstrated that MA harboring the five adaptive mutations and the 5′ UTR and N3H and N5BX regions of JFH-1 (MA/N3H+N5BX-JFH1/5am) could replicate and produce infectious virus efficiently.

Using these novel genotype 2b chimeric viruses, we assessed interferon sensitivity. We found that MA/JFH-1.2/R167G chimeric virus and MA/N3H+N5BX-JFH1/5am virus were more sensitive to interferon than the JFH-1 virus (Fig. 7). Furthermore, we found that MA/N3H+N5BX-JFH1/5am was more sensitive to interferon than MA/JFH-1.2/R167G, indicating that the genetic variation(s) in the NS2, N3P, and NS4A to NS5A regions affect interferon sensitivity. Although genotype 2a viruses are more sensitive to interferon than genotype 2b viruses in clinical studies, JFH-1 displayed interferon resistance in our study.

These results suggest that the JFH-1 regions in the 2b/JFH-1 virus affect the interferon sensitivity of the chimeric virus. Moreover, it was reported that amino acid variations in E2, p7, NS2, and NS5A were associated with the response to peginterferon and ribavirin therapy in genotype 2b HCV infection (10). Therefore, our MA/JFH-1 chimeric virus harboring minimal regions from JFH-1 (MA/N3H+N5BX-JFH1/5am) is more suitable for assessing the characteristics of the MA strain than the MA/JFH-1 chimeric virus, which includes a nonstructural region from JFH-1 (MA/JFH-1.2/R167G). We showed here that replacement of the 5′ UTR and N3H and N5BX regions in MA with those from JFH-1 is able to convert MA into a replicable virus. Using the same strategy, numerous HCV cell culture systems with various genotype 2b strains, as well as genotype 2a strains, may be available.

In conclusion, we established a novel HCV genotype 2b cell culture system using a chimeric genome in MA harboring minimal regions from JFH-1. This cell culture system using the chimeric genotype 2b virus will be useful for characterization of genotype 2b viruses and the development of antiviral strategies.

ACKNOWLEDGMENTS

We are grateful to Tetsuro Suzuki of Hamamatsu University School of Medicine for helpful comments and suggestions. Huh7.5.1 cells were kindly provided by Francis V. Chisari.

A.M. is partially supported by the Japan Health Sciences Foundation and Viral Hepatitis Research Foundation of Japan. This work was partially supported by Grants-in-Aid for Scientific Research from the Japan Society for the Promotion of Science, from the Ministry of Health, Labor and Welfare of Japan, from the Ministry of Education, Culture, Sports, Science and Technology, from the National Institute of Biomedical Innovation, and by Research on Health Sciences Focusing on Drug Innovation from the Japan Health Sciences Foundation.

REFERENCES

1. **Akazawa D, et al.** 2007. CD81 expression is important for the permissiveness of Huh7 cell clones for heterogeneous hepatitis C virus infection. J. Virol. **81**:5036–5045.
2. **Bartenschlager R, Lohmann V.** 2000. Replication of hepatitis C virus. J. Gen. Virol. **81**:1631–1648.
3. **Boulant S, et al.** 2006. Structural determinants that target the hepatitis C virus core protein to lipid droplets. J. Biol. Chem. **281**:22236–22247.
4. **Boulant S, Targett-Adams P, McLauchlan J.** 2007. Disrupting the association of hepatitis C virus core protein with lipid droplets correlates with a loss in production of infectious virus. J. Gen. Virol. **88**:2204–2213.
5. **Choo QL, et al.** 1989. Isolation of a cDNA clone derived from a blood-borne non-A, non-B viral hepatitis genome. Science **244**:359–362.
6. **Gottwein JM, et al.** 2009. Development and characterization of hepatitis C virus genotype 1–7 cell culture systems: role of CD81 and scavenger receptor class B type 1 and effect of antiviral drugs. Hepatology **49**:364–377.
7. **Griffin S, et al.** 2008. Genotype-dependent sensitivity of hepatitis C virus to inhibitors of the p7 ion channel. Hepatology **48**:1779–1790.
8. **Hope RG, McLauchlan J.** 2000. Sequence motifs required for lipid droplet association and protein stability are unique to the hepatitis C virus core protein. J. Gen. Virol. **81**:1913–1925.
9. **Jensen TB, et al.** 2008. Highly efficient JFH1-based cell-culture system for hepatitis C virus genotype 5a: failure of homologous neutralizing-antibody treatment to control infection. J. Infect. Dis. **198**:1756–1765.
10. **Kadokura M, et al.** 2011. Analysis of the complete open reading frame of genotype 2b hepatitis C virus in association with the response to peginterferon and ribavirin therapy. PLoS One **6**:e24514.
11. **Kato T, et al.** 2008. Hepatitis C virus JFH-1 strain infection in chimpanzees is associated with low pathogenicity and emergence of an adaptive mutation. Hepatology **48**:732–740.
12. **Kato T, et al.** 2006. Cell culture and infection system for hepatitis C virus. Nat. Protoc. **1**:2334–2339.
13. **Kiyosawa K, et al.** 1990. Interrelationship of blood transfusion, non-A, non-B hepatitis and hepatocellular carcinoma: analysis by detection of antibody to hepatitis C virus. Hepatology **12**:671–675.
14. **Lindenbach BD, et al.** 2005. Complete replication of hepatitis C virus in cell culture. Science **309**:623–626.
15. **Lohmann V, et al.** 1999. Replication of subgenomic hepatitis C virus RNAs in a hepatoma cell line. Science **285**:110–113.
16. **Masaki T, et al.** 2008. Interaction of hepatitis C virus nonstructural protein 5A with core protein is critical for the production of infectious virus particles. J. Virol. **82**:7964–7976.
17. **Miyamoto M, Kato T, Date T, Mizokami M, Wakita T.** 2006. Comparison between subgenomic replicons of hepatitis C virus genotypes 2a (JFH-1) and 1b (Con1 NK5.1). Intervirology **49**:37–43.
18. **Miyanari Y, et al.** 2007. The lipid droplet is an important organelle for hepatitis C virus production. Nat. Cell Biol. **9**:1089–1097.
19. **Murakami K, Abe M, Kageyama T, Kamoshita N, Nomoto A.** 2001. Down-regulation of translation driven by hepatitis C virus internal ribosomal entry site by the 3′ untranslated region of RNA. Arch. Virol. **146**:729–741.
20. **Murakami T, et al.** 1999. Mutations in nonstructural protein 5A gene and response to interferon in hepatitis C virus genotype 2 infection. Hepatology **30**:1045–1053.
21. **Murayama A, et al.** 2007. The NS3 helicase and NS5B-to-3′X regions are important for efficient hepatitis C virus strain JFH-1 replication in Huh7 cells. J. Virol. **81**:8030–8040.
22. **Murayama A, et al.** 2010. RNA polymerase activity and specific RNA structure are required for efficient HCV replication in cultured cells. PLoS Pathog. **6**:e1000885.
23. **Pietschmann T, et al.** 2006. Construction and characterization of infectious intragenotypic and intergenotypic hepatitis C virus chimeras. Proc. Natl. Acad. Sci. U. S. A. **103**:7408–7413.
24. **Pietschmann T, et al.** 2009. Production of infectious genotype 1b virus particles in cell culture and impairment by replication enhancing mutations. PLoS Pathog. **5**:e1000475.
25. **Scheel TK, et al.** 2008. Development of JFH1-based cell culture systems